

Highlights

Van der Waals Antiferromagnets: From Early Discoveries to Future Directions in the 2D Limit

Rahul Kumar, Je-Geun Park

- Overview of vdW antiferromagnets evolution from 2016 and the future prospects.
- Understanding the crystal structure and magnetism of $TMPS_3$ family members, key players of the vdW antiferromagnetic family.
- Challenges faced while characterizing the vdW magnets in 2D limit and recent advances.
- Review of the new physics unlocked by vdW magnets and their potential use in future spintronics.

Van der Waals Antiferromagnets: From Early Discoveries to Future Directions in the 2D Limit

Rahul Kumar, Je-Geun Park*

Department of Physics and Astronomy, Seoul National University, Seoul, 08826, South Korea

Abstract

The emergence of a long-range magnetic order in the atomically thin, two-dimensional (2D) limit has long remained a fundamental question in condensed matter physics. The advent of exfoliable van der Waals (vdW) materials, particularly transition-metal phosphorus trisulfides ($TMPS_3$; $TM = Fe, Ni, \text{ and } Mn$), provided the first experimental access to this regime and established a foundational platform for investigating 2D magnetism. The 2016 experimental demonstrations of intrinsic magnetism in monolayer $FePS_3$ provided a platform to test key aspects of 2D Ising criticality in the true 2D limit. It was followed by a rapid growth resulting in a wealth of emergent phenomena arising from the interplay of low-dimensional magnetism and quantum materials. We begin this review with the historical development of vdW antiferromagnets and highlight the key physical insights gained over the past decade. We finish with emerging opportunities in which vdW antiferromagnets can serve as versatile platforms for exploring low-dimensional magnetism and its interplay with other quantum degrees of freedom.

Keywords: van der Waals magnets, two-dimensional magnetism, $TMPS_3$, antiferromagnetism, 2D spin models, moiré magnetism, spintronics

1. Introduction — Origin of the Question

Throughout the history of science, materials have often played a central role in advancing the frontiers. New materials open the sealed box of curiosity and imagination, allowing people to ask questions that were previously unimaginable. The discovery of graphene [1] is arguably the watershed moment in 21st century physics that brought the now-vibrant field of 2D materials into being. Subsequently, the question and the idea behind vdW magnets were a natural consequence of these developments in the research of 2D materials [2–4].

As a separate article is dedicated to vdW ferromagnets, we focus exclusively on vdW antiferromagnets here. We encourage readers to consult both articles in parallel to gain a comprehensive perspective on recent developments in the broader landscape of vdW magnets. This article focuses on the historical development and experimental foundations of vdW antiferromagnets.

The isolation of graphene via a simple mechanical exfoliation method assisted by Scotch tape in 2004

[1] demonstrated that atomically thin (truly 2D) materials could be extracted from vdW crystals while retaining their remarkable properties. This breakthrough transformed condensed matter physics and sparked intense efforts to isolate other layered materials such as transition-metal dichalcogenides and hexagonal boron nitride [5, 6]. Because of the simplicity of this approach, scotch tape exfoliation is the widely used technique for peeling a vdW material to a monolayer thickness, which has led to an exponentially growing catalog of vdW materials. Yet, despite this explosive growth, the magnetic analog of graphene received virtually no attention until 2010, when a pivotal question emerged: Does a magnetic vdW crystal analogous to graphene exist?

This material would not only be conceptually compelling, but it would also allow experimental tests of the canonical 2D spin models—Ising [7], XY [8, 9], and Heisenberg [10]—in atomically thin magnetic crystals. These materials could serve as valuable testbeds for investigating 2D magnetism in a range of spin-lattice geometries, including honeycomb [11], triangular [12], and Kagome [13] structures. Figure 1 conceptualizes the 2D magnets within this landscape. Our initial ex-

*jgpark10@snu.ac.kr

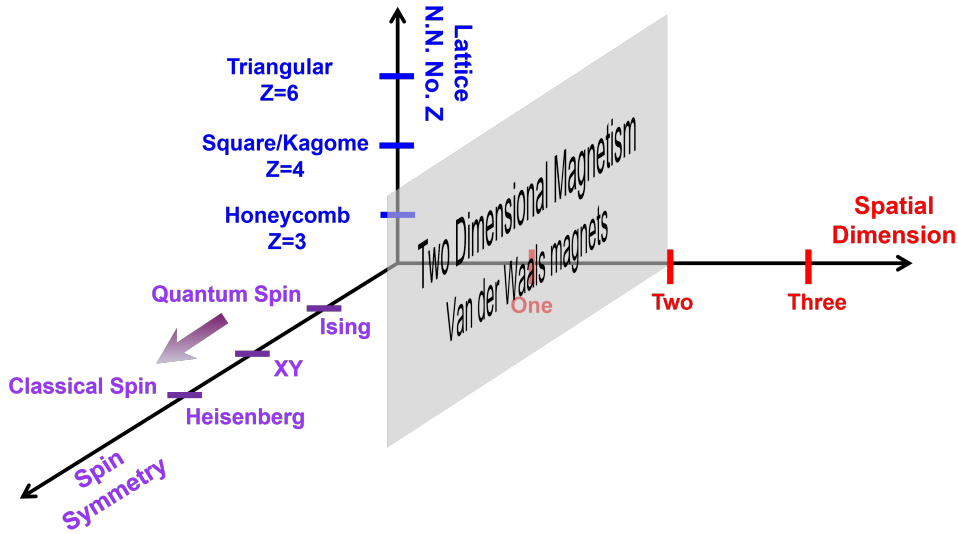


Figure 1: Conceptual landscape of 2D magnets within the three-dimensional space of spatial dimensionality, lattice geometry and spin symmetry.

perimental attempts were made using honeycomb oxides such as Li_2MnO_3 [14], which failed due to strong covalent bonding that prevented easy exfoliation.

The breakthrough came through a systematic literature review, particularly revisiting Brec’s earlier characterization of TMPS_3 [15]. Unlike oxides, TMPS_3 has a weak interlayer bonding, essential for exfoliation, combined with a perfect honeycomb magnetic lattice [16]. Another interesting point is that the TMPS_3 family demonstrated remarkable chemical flexibility with various $3d$ transition-metal ions (Fe^{2+} , Ni^{2+} , Mn^{2+} , etc.) while maintaining a similar chemical structure. Most importantly, it realizes the three fundamental magnetic models: Ising, XY, and Heisenberg. Encouraged by the versatility of this family, Park *et al.* synthesized bulk crystals and demonstrated easy exfoliation down to monolayer FePS_3 [11], NiPS_3 [17], and MnPS_3 [18]. As the original photos show, it was immediately clear that the crystals could be peeled into thin flakes because of their low cleavage energies. The (re)discovery of this family of materials prompted a decade-long research program on vdW magnets that continues to expand today. This decade-long effort has made 2D magnetism a vibrant experimental discipline. Figure 2 provides an overview of the representative vdW magnetic platforms discovered since 2016. This review complements recent comprehensive treatments by focusing on materials trends and experimental phenomenology rather than exhaustive theoretical formalism.

2. Structural and Magnetic Properties of TMPS_3

The TMPS_3 family is a representative material platform, whose physical properties define the essential features and conceptual framework of 2D magnetism. Therefore, a comprehensive understanding of the structural and magnetic characteristics of the TMPS_3 family is necessary before delving into the details of vdW magnetism.

2.1. Crystal structure and the origin of single-ion anisotropy

The TMPS_3 family is distinguished by weak vdW interlayer interactions, enabling reliable mechanical exfoliation down to the monolayer limit. The magnetic ions form a honeycomb lattice within the crystallographic ab plane, with a relatively large separation along the c axis [15, 19]. This quasi-two-dimensional crystal structure, combined with weak interlayer bonding, makes TMPS_3 an ideal platform for investigating magnetic phenomena in the strict 2D limit.

Each transition-metal ion occupies the center of a sulfur octahedron (TMS_6 coordination polyhedron). The crystallographic distortion reduces the local point-group symmetry from cubic (O_h) to trigonal (D_{3d}), leading to a preferred magnetic easy axis or plane. Thus, the magnetic properties of TMPS_3 are governed by a delicate interplay between the crystal electric field and the spin-orbit coupling effects [20]. The resulting single-ion anisotropies can be further affected by the electronic configuration of the transition-metal cation, particularly

Representative Material Platforms of van der Waals Magnets

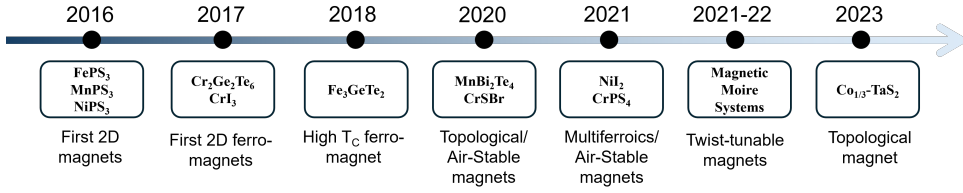


Figure 2: Chronological development of van der Waals magnetic material platforms (2016–2023). The timeline traces major experimental discoveries and their characterization, beginning with the first two-dimensional magnets (FePS₃, MnPS₃, NiPS₃) in 2016, followed by the first ferromagnetic systems (Cr₂Ge₂Te₆, CrI₃) in 2017, and progressing through successive breakthroughs including high-temperature ferromagnets (Fe₃GeTe₂, 2018), topological and air-stable antiferromagnets (MnBi₂Te₄, CrSBr, 2020–2021), multiferroic and air-stable systems (NiI₂, CrPS₄, 2021), twist-tunable magnets (2021–2022), and topological magnets (Co_{1/3}TaS₂, 2023).

when the d -electron configuration retains unquenched orbital angular momentum [20, 21].

2.2. Natural Realization of Canonical 2D Spin Models

A remarkable feature of the $TMPS_3$ family is that different transition-metal cations, despite maintaining an identical crystal structure, exhibit fundamentally different magnetic anisotropies. This flexibility of magnetic symmetry with the same structure is not common among magnetic materials and is an important feature of $TMPS_3$. Crucially, this feature enables direct experimental access to the canonical 2D spin models: Ising, XY, and Heisenberg. This advantage of the $TMPS_3$ platform provides an huge opportunity to explore both dimensionality and symmetry in 2D magnetism, which can control magnetism independently.

2.2.1. FePS₃ (Ising like)

The Fe²⁺ cation ($3d^6$ configuration) has an unquenched orbital angular momentum (${}^5T_{2g}$ state, $L \approx 1$, $S = 2$). With a spin-orbit interaction, this leads to an unusually “giant” easy-axis anisotropy (~ 20 meV) [22, 23], with the magnetic moments pointing strictly perpendicular to the honeycomb layers. The resulting magnetic configuration is effectively equivalent to the canonical 2D Ising model.

2.2.2. NiPS₃ (XY like)

In contrast, the Ni²⁺ cation ($3d^8$ configuration) has a quenched orbital moment (${}^3A_{2g}$ $L = 0$, $S = 1$), such that single-ion anisotropy arises only from weaker second-order perturbative effects mediated by spin-orbit coupling of excited crystal-field states [24, 25]. This weak mechanism generates a moderate easy-plane anisotropy that confines the magnetic moments to the honeycomb ab plane with small canting. The resulting magnetic system is well-described by the 2D XXZ model with

easy-plane anisotropy, commonly referred to as the 2D XY model in the limit of weak out-of-plane anisotropy [26–28].

2.2.3. MnPS₃ (Heisenberg like)

The Mn²⁺ cation ($3d^5$ configuration) features a half-filled d shell with zero orbital angular momentum (${}^6A_{1g}$ $L = 0$, $S = 5/2$), rendering both first- and second-order spin-orbit coupling effects negligible. The resulting magnetic anisotropy is essentially zero, allowing the magnetic moments to point in any spatial direction with equal energy. This near-zero anisotropy [29, 30] allows MnPS₃ to approximate the isotropic 2D Heisenberg model, wherein spin interactions depend only on the relative orientation of neighboring spins rather than their absolute direction. MnPS₃ completes the trio of canonical 2D spin models realized within the $TMPS_3$ family. A summary of the $3d$ orbital splitting and the resulting magnetic anisotropy for all three compounds is shown in Fig. 3.

These properties make $TMPS_3$ one of the few material families where 2D spin models can be experimentally accessed in structurally similar compounds. However, probing these properties in genuinely 2D regimes (monolayer or few-layer) poses a serious experimental challenge. Due to the antiferromagnetic ground state, the total magnetic signal vanishes, except for small canted ferromagnetic moments. This limitation required the development of alternative experimental approaches specifically tailored to probe the antiferromagnetism of $TMPS_3$ in the strict 2D limit. This challenge has driven substantial early innovation in the field and will be discussed in subsequent sections.

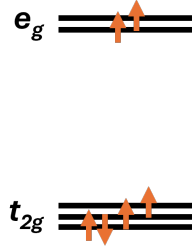
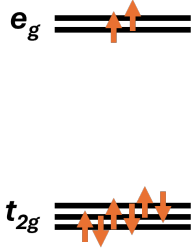
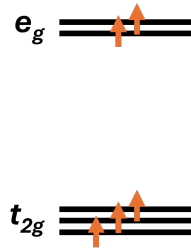
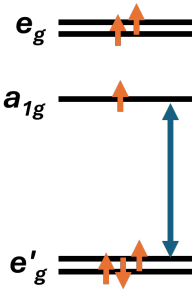
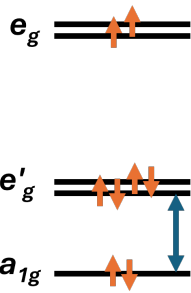
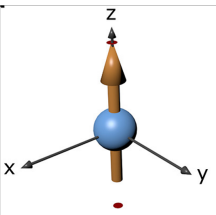
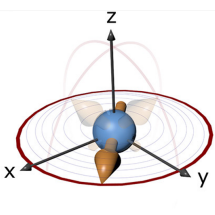
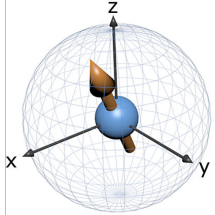
	$FePS_3$	$NiPS_3$	$MnPS_3$
Octahedron			
Trigonal Elongation/ Compression			
Anisotropy			

Figure 3: Crystal field splitting of 3d orbitals and resulting spin anisotropy in transition metal phosphorous trichalcogenides. *Top row*: Octahedral crystal field splitting (e_g and t_{2g} orbitals) for $FePS_3$, $NiPS_3$, and $MnPS_3$. *Middle row*: Trigonal elongation or compression of the octahedral environment, leading to further splitting of the d -orbitals into e'_g and a_{1g} states. The blue vertical arrows qualitatively illustrate the splitting. *Bottom row*: Resulting magnetic anisotropy and spin models. The bottom row illustrations are adapted from [31], Copyright ©2022 The Authors.

3. Overcoming experimental challenges (2012-14)

Exfoliation of the $TMPS_3$ samples introduced additional experimental challenges, including sample handling and the study of magnetism in the truly 2D limit. The sample-handling challenges include charge compensation on the surface and stability under ambient conditions. Given the micrometer-scale lateral dimensions and atomic-scale thicknesses of exfoliated flakes, the available sample volume is too small for conventional bulk characterization techniques such as neutron scattering, superconducting quantum interference device (SQUID) magnetometry, and muon spin relaxation (μ SR). Hence, to study 2D magnetism, a methodological transformation was required, specifically in the field

of optical and electrical probes. The following subsections outline the key experimental challenges and the innovative strategies developed to overcome them.

3.1. Initial sample-dependent challenges

Unlike oxide magnets, vdW magnets, consisting of chalcogenides and halides, are always more sensitive to environmental conditions, which makes proper handling crucial. Bulk flakes of the $TMPS_3$ family are reasonably stable in air, but prolonged exposure (a few hours) to nonideal conditions such as air can easily degrade or damage exfoliated flakes, especially thin ones. Such effects were already reported in the first successful exfoliation study of $NiPS_3$ [17]. Exposure of $NiPS_3$ thin flakes to ambient air led to a pronounced reduction

in optical contrast and Raman intensities over the course of a week.

Furthermore, another serious issue is charge compensation, which may originate from intrinsic or extrinsic defects and can be critical for electronic transport and device performance. We also found that atomic force microscopy measurements of MnPS₃ [18] and NiPS₃ [17] sometimes show a greater height for the monolayer sample (~ 1.5 nm) than the known interlayer spacing (~ 0.6 nm). This is clearly due to the accumulation of water and oxygen adsorbates at the flake-substrate interface. These intrinsic and surface-generated defects are found to cause trouble in achieving unipolar charge carrier behavior and strong optical excitation signatures in early thin-flake studies. To avoid surface degradation and/or contamination, we always handle all exfoliated flakes of the TMPS₃ family in an inert atmosphere, preferably in a glovebox.

3.2. Raman Spectroscopy

Raman spectroscopy has provided unprecedented access to magnetism in 2D materials beyond thickness determination [32, 33] because of its ability to detect quasi-particles arising from changes in the spin structure. The non-invasive nature and surface sensitivity of Raman spectroscopy make it particularly powerful for probing magnetic systems. This capability is especially important for antiferromagnets, which possess a net-zero magnetic moment, thereby rendering alternative techniques, such as those based on the magneto-optic Kerr effect, ineffective. Another interesting point, not well-appreciated before, is the fact that net long-range magnetic ordering (ferromagnetic or antiferromagnetic) scatters incident light inelastically, as established in the pioneering theoretical work of Fleury and Loudon [34]. These magnetic excitations can modulate phonon modes, which Raman measurements readily detect. A representative case of probing thickness-dependent magnetism in FePS₃, which is one of the first vdW magnets studied in the truly 2D limit, is detailed in the following.

Temperature-dependent polarized Raman measurements were performed down to 10 K on FePS₃ samples of varying thicknesses. To identify the magnetic transition temperature, the fundamental principle of Raman spectroscopy was exploited: it can probe energy excitations arising from symmetry breaking. Upon magnetic ordering, rotational symmetry is broken, leading to the emergence of magnons, the quanta of spin-wave excitations. The room-temperature Raman spectra of FePS₃ reveal six phonon modes, of which the low-frequency modes P₁ and P₂ primarily comprise iron vi-

brations [35]. Below the magnetic transition temperature, spin ordering induces pronounced changes in these modes, as depicted in Fig. 4(a). This change arises from Brillouin zone folding resulting from zig-zag antiferromagnetic ordering, which maps the *M* point (from the paramagnetic state) onto the Γ point, thus making zone-boundary phonons Raman-active [36–38]. This spectroscopic signature correlates excellently with the magnetic transition observed in the susceptibility data (Fig. 4(b)), which further indicates Ising-type anisotropy. However, the peak intensities of the higher-energy modes remain unchanged, as shown in Fig. 4(c), reflecting predominantly molecular-like vibrations from the (P₂S₆)⁴⁻ bipyramidal structures. Although Raman spectroscopy constitutes a powerful tool for probing magnetism through magnon modes [39] and spin-lattice coupling [40], it provides only qualitative information and cannot quantitatively determine the magnetic order parameter or elucidate the underlying spin structure.

3.3. Second Harmonic Generation

Another optical tool that has proven particularly useful for vdW antiferromagnets is second-harmonic generation (SHG). SHG relies on a nonlinear optical process and has been widely used to detect broken inversion symmetry in a given system. For example, when a system undergoes a ferroelectric transition, the SHG is a useful tool to determine the broken inversion symmetry. Likewise, it can be an ideal tool for measuring a similar inversion-breaking effect due to magnetic transitions.

MnPS₃ undergoes an antiferromagnetic transition at 78 K, and the type I Néel phase breaks the inversion symmetry, unlike FePS₃ and NiPS₃ [41]. The pronounced SHG signal observed in MnPS₃ is in stark contrast to that obtained from Raman studies of the same material, which exhibit certain hints of magnetic ordering. However, it is not easy to connect the observed anomaly of the Raman data directly to the magnetic ordering [42]. Another notable case is the study of NiI₂, the first vdW multiferroic system [43, 44]. In both cases, SHG has been crucial for determining the magnetic phase transition and, consequently, the multiferroic properties down to the bilayer and monolayer, respectively.

3.4. Optical Linear Dichroism

Although Raman spectroscopy and SHG measurements can identify magnetic phase transitions and symmetry breaking, they do not have the spatial resolution needed to map the antiferromagnetic domains. Optical linear dichroism, which measures the differential absorption or reflectance of two orthogonally polarized

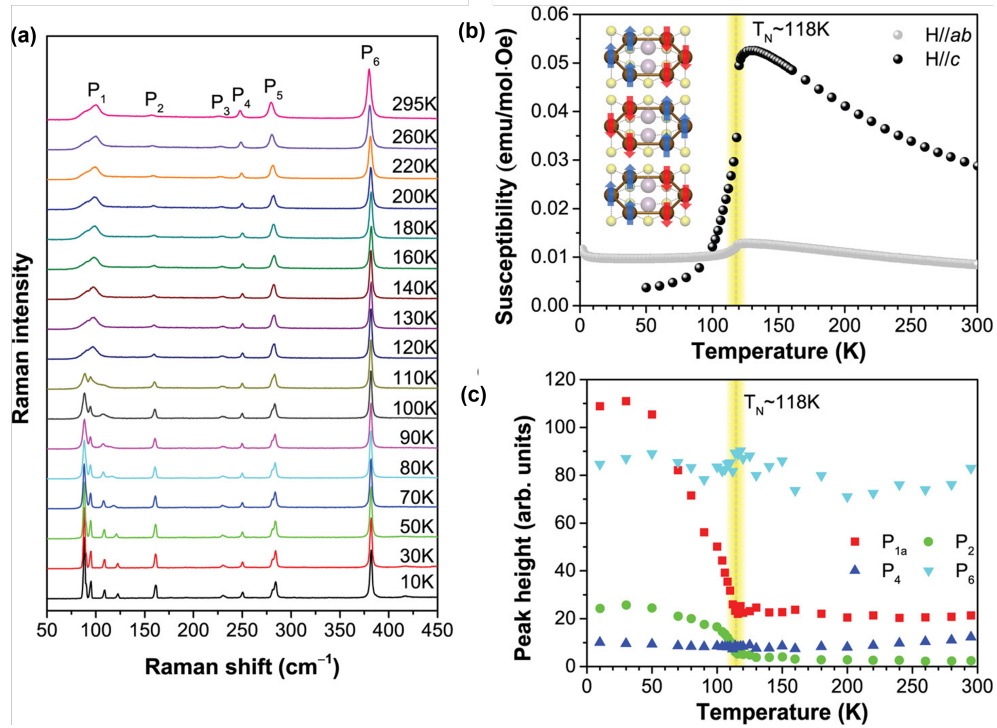


Figure 4: Temperature-dependent Raman spectroscopy and magnetic characterization of bulk FePS₃. (a) The temperature dependence of the Raman spectrum from 10 K to 295 K reveals six phonon modes; low-frequency modes P₁ and P₂ (iron vibrations) exhibit pronounced intensity changes across the magnetic transition, whereas higher-energy modes remain relatively stable. (b) Magnetic susceptibility measured along the *ab*-plane (black spheres) and *c*-axis (gray spheres) exhibits a sharp transition at $T_N \approx 118$ K, with the inset showing zig-zag antiferromagnetic alignment of Fe moments. (c) Low-frequency Raman modes (P_{1a} and P₂) exhibit dramatic intensity increase below T_N . In contrast, higher-energy modes remain temperature-independent, confirming that magnetic ordering induces Brillouin zone folding and couples magnetic and vibrational excitations. The figure is adapted from [11].

lights, addresses this limitation by probing the electronic anisotropy induced by the magnetic order. Unlike the linear magneto-optical effect, which scales linearly with magnetization, linear dichroism scales with the square of the magnetic order parameter, making it more effective for antiferromagnets.

FePS₃ is one such example that exhibits giant optical linear dichroism due to electronic anisotropy linked to the orientation of zigzag chains. Further, angle-dependent linear dichroism measurements can distinguish the three possible zigzag directions [45]. Similarly, linear dichroism has been employed for CrCl₃, which is an in-plane antiferromagnet, to determine the in-plane Neel vector orientation and spin-flop transitions under the applied magnetic fields [46].

3.5. Advances in magnetic probes

Although these optical tools are quite handy, one needs local probes to further explore the microscopic physics of these vdW magnets. One requirement is that these probes have a spatial resolution smaller than the

characteristic length scale of observables such as magnetic domains and non-collinear spin orders, thereby ensuring accurate resolution of intrinsic magnetic properties. Therefore, a careful selection of the magnetic probe is essential as the specific physical quantities being measured often render certain techniques more suitable for particular systems.

Magnetic force microscopy (MFM), introduced in the 1980s as an extension of atomic force microscopy, represents one such technique. The MFM primarily detects the Lorentz force between a ferromagnetic-coated cantilever tip and the stray magnetic field emanating from the sample. MFM cantilevers are typically manufactured with spring constants comparable to those of atomic bonds, resulting in a high spatial resolution (~ 50 nm) [49, 50]. However, the mechanical resonance frequency of the cantilever imposes a fundamental upper limit on measurable spin dynamics, restricting the bandwidth to approximately tens of hertz [51]. Serri *et al.* [47] demonstrated MFM's applicability to the vdW

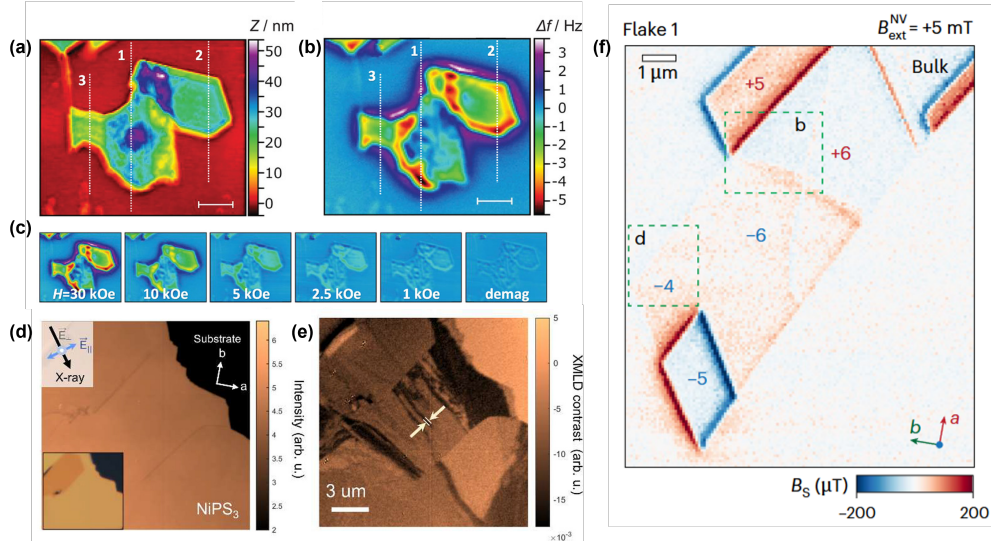


Figure 5: (a) Atomic force microscopy (AFM) image of exfoliated CrCl_3 flakes on silicon substrate with numbered profiles (1, 2, 3) indicating regions of quantitative analysis. (b) Corresponding magnetic force microscopy (MFM) image acquired at 50 kOe and 14 K, revealing clear magnetic contrast that correlates with flake thickness; dotted lines denote the same profiles as in (a) for direct comparison. (c) Sequence of MFM images acquired at 14 K under progressively decreasing magnetic fields (30 kOe, 10 kOe, 5 kOe, 2.5 kOe, 1 kOe, and demagnetized state), demonstrating field-dependent magnetization reversal. (d) Normalized X-ray photoemission electron microscopy (X-PEEM) image of a 48 nm thick NiPS_3 flake recorded at 70 K with photon energy 850.2 eV; the upper inset shows the X-ray incidence direction and electric field polarization geometry, while the lower inset displays the corresponding optical microscope image. (e) X-ray magnetic linear dichroism (XMLD) asymmetry map of the same region, revealing the spatial distribution of magnetic anisotropy and spin orientation. (f) Stray magnetic field (B_S) image mapping the nanoscale spin texture; the top and bottom five-layer regions exhibit opposite magnetization states ($|+5\rangle$ and $|-5\rangle$), while the intervening even-layer region displays a weak field signature indicative of antiphase domain walls between $|+6\rangle = \uparrow\downarrow\uparrow\downarrow$ and $|-6\rangle = \downarrow\uparrow\downarrow\uparrow$ configurations. Panel (a)-(c) are adapted from [47], Copyright ©2020 WILEY-VCH Verlag GmbH & Co. KGaA, Weinheim, panels (d) and (e) are from [24], and panel (f) is from [48], Copyright ©2025 Nature publications.

antiferromagnet CrCl_3 , observing clear magnetic contrast in flakes with thicknesses ranging from 10 to 50 nm at 14 K under an applied field of 50 kOe, as indicated in Fig. 5(a) and (b). The magnetic signal faded with decreasing field strength, and analysis of contrast profiles revealed that saturation magnetization remains independent of layer number within this thickness regime, as can be clearly seen in Fig. 5(c).

X-ray magnetic linear dichroism (XMLD) is a complementary experimental tool. When combined with X-ray photoemission electron microscopy (X-PEEM), it provides atomic-scale monolayer sensitivity and nanometer spatial resolution [22, 52–54]. XMLD exploits the differential absorption between orthogonal linear polarizations (e.g., horizontal versus vertical) in magnetic systems, making it particularly powerful for detecting antiferromagnetic order, non-collinear spin structures, and magnetic anisotropy despite zero net magnetization. XMLD-PEEM measurements have recently been used to image thermally fluctuating Néel vectors in NiPS_3 [24]. The measurements performed at 70 K on a 48 nm thick flake successfully mapped stripe-

like magnetic domains with characteristic dimensions of approximately 200 nm, providing direct access to the Néel vector orientation, as exhibited in Fig. 5(e) corresponding to the optical image presented in Fig. 5(d) [24].

However, scanning nitrogen-vacancy (NV) center microscopy (SNVM) has recently gained substantial interest for imaging various van der Waals magnets. This technique leverages diamond NV centers, which function as single-spin scanning sensors [55], with magnetic measurements carried out by optically detected magnetic resonance (ODMR) spectroscopy [56]. In this approach, the electron paramagnetic resonance spectrum of the defect center is recorded while the probe is maintained in proximity to the sample surface. SNVM achieves a spatial resolution of approximately 20 nm [57, 58] combined with an impressive magnetic sensitivity of $\sim 100 \text{ nT Hz}^{-1/2}$ [59], which makes it ideal for probing domain structure and quantifying magnetic strength in vdW antiferromagnets. Furthermore, SNVM can also perform spin relaxometry in the NV resonance region (GHz frequencies) [60–62], which can be

extended to kHz-MHz ranges using dynamical decoupling sequences [63, 64]. Wang *et al.* [48] employed SNVM to reveal antiferromagnetic and ferromagnetic-like regions in CrPS₄, corresponding to even and odd layer configurations (see Fig. 5(f)). Additionally, they demonstrated nanoscale magnetization switching, thereby establishing SNVM as a powerful magnetic characterization tool.

4. Early developments: talks and papers

4.1. Two public presentations

The question of whether magnetism could be stabilised in a true vdW monolayer was notably highlighted by our group at the Korean Physical Society (KPS) meeting in 2015 [65]. Over the past many decades, the Mermin–Wagner theorem [10] has been a primary source of skepticism regarding experimental attempts to observe 2D magnetism, as it was rigorously established as a fundamental theorem in the late 1960s that long-range magnetic order is forbidden in 2D systems with continuous symmetries. However, Onsager’s seminal solution of the 2D Ising model [7] showed that discrete symmetries and pronounced magnetic anisotropy can circumvent this constraint, enabling stable magnetic ordering at finite temperatures. This theoretical insight suggested that 2D magnets with Ising-type anisotropy might evade the apparent prohibition against ordered states in reduced dimensions. The rise of 2D materials after the discovery of graphene has made the question impossible to ignore. Although the question appeared simple and interesting, it was not easy for one to foresee that its answer could open a new frontier in 2D physics and substantially advance spintronics and quantum device engineering.

The presentation at the KPS fall meeting in 2015 caused a stir among those who attended, although it was still localized at the time. Subsequent presentations at the Japan–Korea–Taiwan Workshop [66] brought attention to a wider community, sharing both intellectual challenges and motivations. This concerted effort strengthened the position of transition-metal phosphorus trisulfides, $TMPS_3$ ($TM = Mn, Fe, Co, Ni$), as a promising platform for realizing 2D magnetism. These official presentations conveyed to the community that, with a suitable experimental framework, the still-nascent field of 2D vdW magnets can be advanced through rigorous studies.

4.2. Four Papers

In 2016, four key early papers from our group established exfoliation protocols and provided the first

monolayer-scale evidence for antiferromagnetic order. In a work of NiPS₃ [17], Kuo *et al.* demonstrated the first successful mechanical exfoliation of the vdW magnet, NiPS₃, to the monolayer limit using the conventional scotch-tape methodology. The authors employed optical contrast, Raman spectroscopy, and atomic force microscopy to identify flakes and determine the number of layers with precision. In particular, tracking the out-of-plane sulfur mode, $A_{1g}^{(1)}$, provided qualitative layer identification. Although no direct magnetic measurements were reported, this work established $TMPS_3$ as a versatile platform for 2D magnetism. The chemical flexibility of this family, as mentioned above, combined with the possibility of substituting sulfur with selenium, has created a rich playground for exploring 2D magnetic phenomena.

Building on this success, our group subsequently investigated MnPS₃, another $TMPS_3$ family member that is amenable to monolayer exfoliation, employing conductive atomic force microscopy (C-AFM) for transport characterization [18]. Tunneling transport measurements were conducted on MnPS₃ flakes ranging from monolayers to tens of layers deposited on a 70 nm indium tin oxide (ITO) layer on a silicon substrate. These measurements conclusively confirmed the insulating character of MnPS₃ in all thicknesses down to the monolayer limit, thereby extending the scope of magnetic tunnel junction research to encompass 2D magnetic materials.

In the same year, our group also turned its attention to FePS₃, conducting comprehensive magnetism measurements in the truly 2D limit using Raman spectroscopy as the primary probe [11]. As detailed in the preceding Raman spectroscopy subsection, Raman measurements unambiguously confirmed long-range magnetic ordering that persists down to the monolayer limit in FePS₃. This result provided experimental verification of Onsager’s solution [7] for 2D order-disorder transitions: while the Mermin–Wagner theorem [10] forbids long-range ordering in XY and Heisenberg models at finite temperatures in reduced dimensions, Onsager demonstrated that 2D Ising systems can sustain long-range magnetic order at finite temperatures. This work thus constituted the first atomically thin, exfoliable vdW magnet (monolayer). Figure 6 presents a unified summary of the three seminal studies, showing the magnetic structures and the minimum exfoliated thickness.

During the discoveries of antiferromagnetism, ferromagnetic ground states were reported in Cr₂Ge₂Te₆ [68] and CrI₃ [69] in 2017, establishing that 2D vdW magnets could exhibit both conventional long-range order. The demonstration of both magnetic states

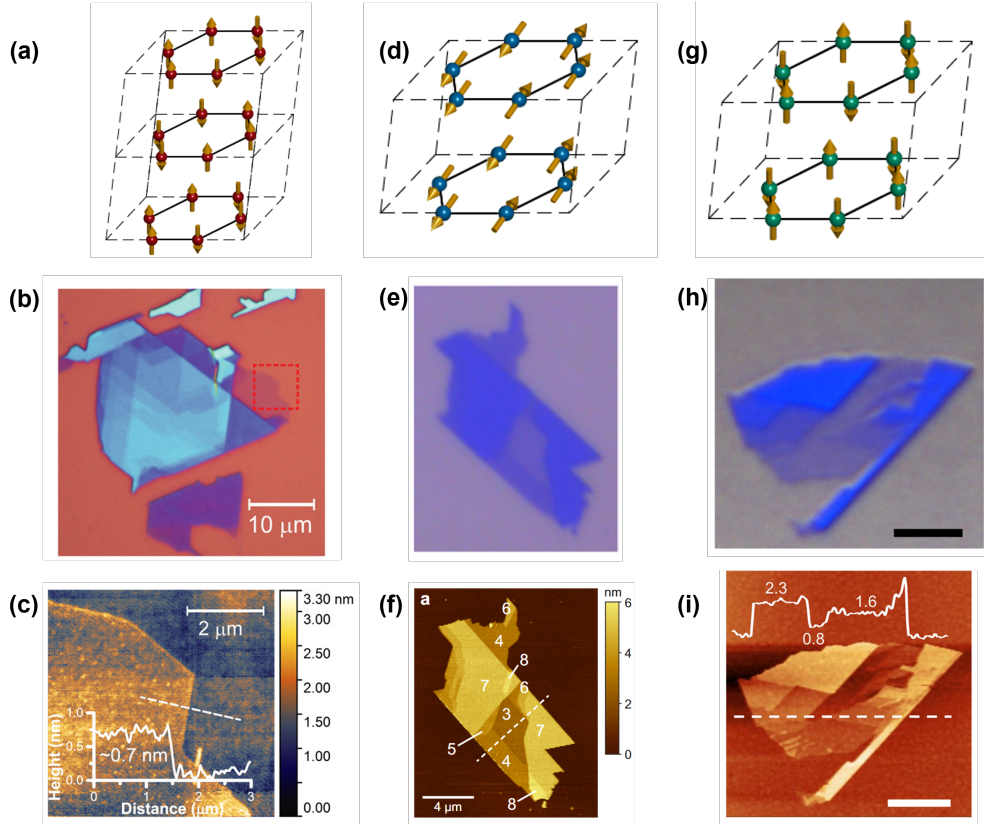


Figure 6: (a) Ising-type antiferromagnetic ground state of FePS_3 . (b-c) Optical contrast image and atomic force microscopy topography of monolayer FePS_3 on SiO_2/Si substrate, confirming successful mechanical exfoliation to the single-layer limit. (d) XY-type antiferromagnetic configuration of NiPS_3 . (e-f) Brightfield optical microscopy and corresponding tapping-mode AFM topography of thin NiPS_3 sheets with layer numbers (3–8 layers) clearly identified from height analysis. (g) Heisenberg-type antiferromagnetic spin structure of MnPS_3 . (h-i) Optical microscopic and AFM topographic images of MnPS_3 flakes ranging from monolayer to hexalayer, with quantitative height profiling revealing the progressive increase in thickness and corresponding structural features. Panel (a), (d) and (g) are adapted from [67]; panels (b-c) are from [11]; panels (e-f) are from [17] and panels (h-i) are from [18].

caused a global research surge in 2D magnetism, rapidly expanding the field to encompass novel phenomena such as spin-filtering in CrI_3 tunnel barriers [70, 71], gate-tunable magnetism [72], and the emergence of 2D magneto-optical effects. International participation expanded dramatically across multiple research frontiers, and heterostructure engineering (graphene, transition-metal dichalcogenides, moiré superlattices) has emerged as one of the most prominent directions [73–75].

This explosive growth in the field was articulated in the seminal viewpoint by Park [4], who articulated the opportunities and challenges of 2D magnetic vdW materials, posing the question: “magnetic graphene?” This perspective further recognised the transformative potential of 2D magnetism for fundamental physics and technological applications, solidifying vdW magnets as a central pillar of contemporary condensed-matter re-

search.

5. New physics enabled by 2D magnets

5.1. Dimensional crossover and magnetic criticality

In the 2D limit, there are three principal mechanisms of magnetic ordering. They are (1) magnetic anisotropy, (2) dipolar interactions, and (3) competing exchange pathways. First, magnetic anisotropy suppresses the logarithmic divergence of thermal fluctuations predicted by the Mermin–Wagner theorem [10]. Second, dipolar interactions, although weak, stabilize long-range order and reinforce anisotropy effects. Finally, competing exchange pathways enable tunable control over magnetic properties.

Magnetic anisotropy arises from the interplay between crystal-field splitting and spin-orbit coupling,

thereby establishing spin structures with preferred orientations. For example, FePS₃ exhibits large single-ion anisotropy (~ 20 meV), which stabilizes Ising-type antiferromagnetic order with an easy out-of-plane axis [22]. This dimensional reduction of spin space from three to one profoundly suppresses thermal fluctuations. In contrast, the relatively weak single-ion anisotropy in NiPS₃ [76] and CoPS₃ [77] leads to XY-type antiferromagnetic order, confining spins to a single plane.

Dipolar interactions have been proposed as a key stabilizing mechanism for the long-range antiferromagnetic order in NiPS₃ monolayers. Theoretical studies reveal a complex exchange interaction hierarchy [21]: the nearest-neighbor coupling is ferromagnetic (~ -2.5 meV), the second nearest-neighbor interaction is weakly antiferromagnetic (~ 0.2 meV), and the third nearest-neighbor coupling is strongly antiferromagnetic (~ 13.9 meV), with the latter dominating the ground state [28]. This exchange frustration suggests that dipolar interactions having magnitudes comparable to exchange parameters may provide essential long-range coherence and anisotropic stabilization that complement single-ion anisotropy in the monolayer limit [21].

The exchange pathways further illuminate the role of the bond geometry and electronic configuration in stabilizing magnetic order. For example, MnPS₃ magnetism is dominated by nearest-neighbor interactions originating from t_{2g} orbital magnetism [29, 30, 78]. By contrast, NiPS₃ exhibits third nearest-neighbor exchange as the strongest interaction, a consequence of the filled t_{2g} subshell and strong hybridization between the $d_{x^2-y^2}$ orbitals and sulfur p -orbitals within the same atomic layer [78]. These distinct exchange hierarchies yield fundamentally different ground states, the Néel order in MnPS₃ versus the zig-zag order in NiPS₃, accompanied by widely separated magnetic transition temperatures (78 K versus 155 K), demonstrating how subtle variations in electronic structure encode dramatic consequences for 2D magnetism.

5.2. Optical control of magnetic anisotropy

In 2D magnets, magnetic anisotropy not only dictates spin ordering geometry but also protects magnetic order from thermal fluctuations, which intensify with dimensional reduction. This intricate coupling between magnetic order and anisotropy motivates the development of strategies to dynamically control anisotropy, thereby providing unprecedented access to manipulate magnetic ordering. As described in section 2, the strength of magnetic anisotropy is generally determined by the coupling between the electronic orbital angular momentum and spin. However, most 2D magnets

based on transition-metal ions possess partially or fully quenched orbital angular momentum [25]. One powerful approach to controlling magnetic anisotropy is optical pumping to higher-energy orbital states [79–82]. For example, FePS₃ exhibits an unquenched orbital moment ($L \sim 1$), allowing anisotropy control through optical resonance of low-energy magnon and phonon modes to higher amplitudes. This nonlinear driving of specific phonon modes modifies in-plane distances between magnetic ions, establishing a metastable state (see Fig. 7(a–b)) with an impressive lifetime of 2.5 milliseconds [83].

On the other hand, in systems with zero or negligible unquenched orbital angular momentum, magnetic anisotropy arises from spin-orbit-driven mixing of the ground state with higher-energy states bearing residual orbital character. For example, NiPS₃ has a quenched orbital moment ($L = 0$), and magnetic anisotropy emerges from spin-orbit-mediated hybridization of the ground state (${}^3A_{2g}$) with the first excited state (${}^3T_{2g}$) [20, 84]. In such cases, magnetic anisotropy can be controlled by resonating photon energy with orbital transitions among crystal-field-split levels, as depicted in Fig. 7(c–d). These magnon modes, activated by subterahertz frequencies, are used to perform polarization-dependent control of the magnon amplitude, confirming the dynamic manipulation of magnetic anisotropy [25].

The weak magnetic anisotropy (~ 0.009 meV) of MnPS₃ is due to the mixing of the ground state (${}^6A_{1g}$) with excited states bearing a residual orbital character. A recent control of magnetic anisotropy in this system employs a Floquet method [85, 86], which bypasses the issue of heating by using subgap wavelengths. Shan *et al.* [87] showed that optical pumping of MnPS₃ at subgap frequencies ($\hbar\omega = 0.66$ – 0.99 eV) resonant with crystal-field transitions hybridizes the ground state and charge-transfer states through a time-dependent oscillating field ($\sim 10^9$ V/m), (see Fig. 7(g–j)). This dynamic modulation of the crystal field modulates the spin-orbit admixture coefficients, allowing real-time control of both the strength and orientation of the magnetic anisotropy measured by SHG.

5.3. Moiré magnetism: Stacking angle engineering

An alternative pathway to unlock tunable magnetism in vdW magnets exploits stacking-angle engineering through moiré superlattices created by rotating or translating individual 2D magnetic layers relative to each other. In particular, small stacking angles can result in various stacking geometries that cannot be realized in a pristine sample. The presence of these high-symmetry configurations with distinct interlayer

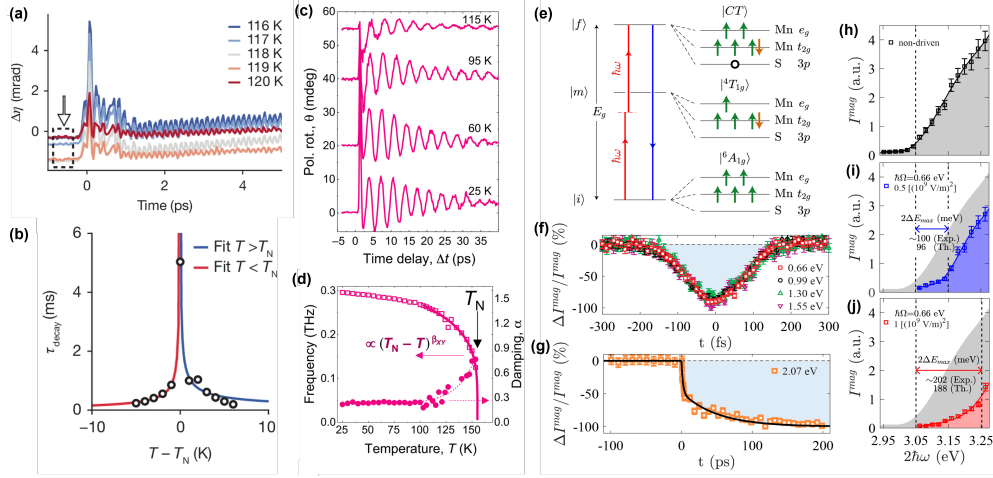


Figure 7: (a–b) FePS₃: Pre-time-zero ellipticity signal near the Néel temperature reveals metastable-state formation; decay-time analysis demonstrates critical exponent behavior ($z\nu = 0.89$ above T_N and 0.56 below T_N), indicative of magnetic criticality. (c–d) NiPS₃: Temperature-dependent time-resolved polarization rotation following 1.08 eV pump excitation exhibits pronounced oscillations; the extracted magnon frequency follows a power law $\propto (T_N - T)^{\beta_{kv}}$, demonstrating magnon softening at the magnetic transition. (e) Schematic energy diagram for resonant electric-dipole second-harmonic generation (ED-SHG) in MnPS₃: multi-electron states (left) and corresponding orbital/spin configurations (right) illustrate the hybridization of ground (${}^6A_{1g}$) and charge-transfer states ($[CT]$) under optical driving. (f) Transient SHG response ($\Delta I_{\text{mag}}/I_{\text{mag}}$) for subgap pump photon energies ($\hbar\omega = 0.66$ – 1.55 eV) at fixed electric-field amplitude ($E_{\text{max}} = 10^9$ V/m). (g) SHG transient under resonant pumping conditions at photon energy 2.07 eV. (h–j) Non-driven (h) and pump-driven SHG spectra at $t = 0$ for increasing field amplitudes (i) $(E_{\text{max}})^2 = 0.5 \times 10^{18}$ V²/m² and (j) 1.0×10^{18} V²/m², demonstrating field-dependent modification of the anisotropic response and validating the Floquet mechanism for dynamic control of spin-orbit admixture. Panels (a–b) are adapted from [83], panels (c–d) are from [25] and panels (e–j) are adapted from [87].

exchange interactions provides an additional control parameter [73, 74, 88]. The bilayer CrI₃ is an archetypal antiferromagnet for such stacking engineering in which exchange interactions and the resulting magnetic state depend on the type of stacking, whether it is monoclinic (AB') or rhombohedral (AB) stacking [89]. This results in a noncollinear spin structure that exhibits in-plane spin canting, with magnetic order perpendicular to the plane, which can be further classified as bubble-like excitations or magnetic skyrmions.

5.4. Magnetic heterostructures

One notable trend in recent work on vdW magnets is the study of their heterostructures with 2D conductors and semiconductors. A large volume of recent work has focused on proximity effects, aiming to realize new functional capabilities for future device applications [90]. A clear strategy has been the use of heavy metals, such as tungsten (W) or platinum (Pt), which possess strong spin-orbit coupling [91–93]. In this configuration, the heavy metals can be used to enhance the effectiveness of magnetization detection probes for antiferromagnets. If successful, it could circumvent the challenges posed by zero net magnetization and the inherent limitations of conventional detection techniques. In this regard, it should be noted that Ma *et al.* demon-

strated substantial spin polarization in the Pt layer of FePS₃ / Pt heterostructures, resulting in a measurable anomalous Hall effect [94]. Furthermore, the temperature dependence of the anomalous Hall response reproduces the magnetic phase transition of FePS₃, providing elegant proof of proximity-induced magnetization transfer.

A particularly promising recent development involves the manipulation of the topological state using ionic gating, as reported for Co_{1/3}TaS₂, an air-stable intercalated non-coplanar antiferromagnet with intrinsic topological spin texture [95]. Zhang *et al.* [96] further demonstrated control of topological spin chirality in Co_{1/3}TaS₂ by integrating it with Pt, which leads to spin-Hall-effect-induced nonvolatile and reversible switching. Interestingly, Co_{1/3}TaS₂ exhibits an intrinsic self-spin orbit torque arising from broken inversion symmetry and pronounced Berry curvature hotspots, enabling field-free and heavy-metal-free electrical switching of topological spin chirality. This dual-pathway approach, which combines interfacial spin-orbit torque or intrinsic self-spin-orbit torque, establishes new paradigms for topological spintronics and quantum magnetic device engineering.

Exchange bias effects, which emerge at the ferromagnetic/antiferromagnetic interfaces, represent an-

other important avenue for heterostructure engineering and manipulation for spintronics applications [97–99]. Recently, Albarakati *et al.* demonstrated that the exchange field in $\text{FePS}_3/\text{Fe}_3\text{GeTe}_2$ heterostructures can be dynamically controlled using solid protonic gating, allowing electrical modulation of interfacial magnetic coupling [100]. The exchange bias field can also be tuned by changing the thickness of the ferromagnet, as reported for $\text{Fe}_{5-x}\text{GeTe}_2/\text{CrPS}_4$ heterostructure [101]. Moreover, X. Wang *et al.* have shown pressure control of emergent interfacial antiferromagnetism in $\text{Fe}_3\text{GeTe}_2/\text{MnPS}_3$ heterostructure, which goes beyond the conventional effect of exchange bias [102].

Magnetoresistance, defined as a change in electrical resistance on application of a magnetic field, can also provide key insights into the interfacial physics. For instance, in the case of the $\text{MnPS}_3/\text{Fe}_3\text{GeTe}_2$ heterostructure, three distinct resistances are observed as a possible consequence of unsynchronized magnetic switching between the antiferromagnetic layer and ferromagnetic interface and bulk of the ferromagnet [98]. A large negative magnetoresistance is reported in CrSBr, a layered antiferromagnet, which can be tuned by gating [103, 104]. Moreover, twisted bilayers of CrSBr exhibit a tunneling magnetoresistance exceeding 700 %, indicating their potential for high-storage spintronic devices [105]. Similarly, a nonvolatile but multistate magnetoresistance has also been observed in $(\text{Fe}_{0.8}\text{Co}_{0.2})_3\text{GaTe}_2/\text{WSe}_2/(\text{Fe}_{0.8}\text{Co}_{0.2})_3\text{GaTe}_2$, where $(\text{Fe}_{0.8}\text{Co}_{0.2})_3\text{GaTe}_2$ is an A-type antiferromagnet with a transition temperature around 210 K [106]. Interestingly, another A-type antiferromagnet, CrPS₄, shows oscillatory magnetoresistance which is intrinsic in nature and may be due to a canted magnetic state under applied magnetic fields [107].

6. Toward 2D Spintronic and Quantum Devices

Ferromagnetic materials have traditionally been heavily used in spintronics devices. However, the increasing demand for low-power consumption devices, high storage density, and faster read/write speeds has recently caused renewed interest in alternative antiferromagnetic platforms [108–110]. In this recent context, antiferromagnets promise several advantages over ferromagnets: for example, ultrafast spin dynamics, robustness against external magnetic fields, and negligible stray-field radiation [111, 112]. Among antiferromagnets, there are two different classes: one with collinear spin structures and another with non-collinear spin textures.

A recent example of such collinear antiferromagnets is CrSBr, an A-type collinear antiferromagnet that exhibits intrinsic net-zero spin polarization [113–115]. Carrier doping is shown to modify the interlayer exchange coupling and stabilize a highly spin-polarized ferromagnetic phase. For example, the magnetic order of CrSBr could be spatially modulated by combining a doping approach with local interfacial charge transfer from graphene contacts. An interesting point is that the resulting lateral FM/AFM/FM configurations are, in principle, gate-tunable spin valves with a complete reversal of spin polarization across a critical gate voltage without requiring ferromagnetic metal contacts [116]. This represents a major simplification with respect to the integrated device architectures of conventional spintronics. However, the inherent unresponsiveness of antiferromagnets to external magnetic perturbations remains a significant technical challenge for controlling and probing magnetic order.

At the same time, non-collinear antiferromagnets offer a potential solution by synergistically combining the advantages of ferromagnets (efficient reading and writing through detectable magnetization) with those of antiferromagnets (ultrafast dynamics, negligible stray fields, and intrinsic non-volatility) while simultaneously circumventing their respective drawbacks. Two such candidates are $\text{Ni}_{1/3}\text{NbS}_2$ and $\text{Co}_{1/3}\text{TaS}_2$. In the case of $\text{Ni}_{1/3}\text{NbS}_2$, the application of an in-plane current leads to the generation of antiferromagnetic spin-orbit torque, which then acts as a controller of the entire helical order [117]. Meanwhile, in the case of $\text{Co}_{1/3}\text{TaS}_2$, controlling its topological $3Q$ state, which manipulates the associated spontaneous topological Hall effect, can open new pathways for the efficient readout of antiferromagnetic states electrically [118, 119]. Furthermore, Meng *et al.* have demonstrated successful integration with the dichalcogenide MoS_2 , revealing its potential for future spintronic devices [120].

7. Outlook and future prospects

In the case of 2D materials, vdW magnets will further strengthen their position as building blocks, especially through interface engineering and light-matter interaction, in the upcoming decade. The vdW magnets can be considered as an intersection space of nanoscale condensed matter physics and spintronics. The exploration of this space will advance our existing understanding of nanoscale magnetism and how these could be utilized for next-generation practical devices. As illustrated in Fig. 8, when vdW magnets are combined with properties such as superconductivity, topology, or multifer-

roicity, referred to as 'quantum cards', individually or in combination, novel emergent phenomena that were previously inaccessible can be studied.

7.1. Robustness of bulk properties in 2D limit

First of all, we would like to emphasize an important aspect which is often overlooked: whether a vdW magnet retains its bulk properties down to the exfoliated limit. Generally, properties in the thin limit remain the same as in bulk, but one should be careful when interpreting results in the 2D limit. For instance, a few-layer CrI₃ favours a monoclinic stacking and hence an antiferromagnetic ground state, while it has a ferromagnetic ground state in bulk form owing to the rhombohedral stacking [121, 122]. Similarly, one should be careful about the potential substrate effects which may contribute to their magnetic properties. Hence, it is necessary to do structural scrutiny also to confirm that the observed phenomena are intrinsic in nature.

7.2. Beyond Three Fundamental Spin Models in the 2D Limit

The discovery of vdW antiferromagnets has enabled the experimental realization of Ising, XY, and Heisenberg spin models with unprecedented tunability and control. These systems are expected to enable the further exploration of exotic spin phases, such as spin-glass [123] and spin-liquid states [124], in the 2D limit. However, such disordered phases, characterized by quenched disorder, frustration, and the absence of long-range order, remain largely unexplored in vdW systems. A fundamental open question is whether the spin-glass or spin-liquid phases retain stability when reduced to the 2D limit [125].

In the case of spin-glass states, theoretical studies indicate that, although the 2D random Ising model lacks a finite-temperature transition, it may host a zero-temperature spin-glass transition at or above two dimensions [126]. For XY and Heisenberg spin glasses with short-range interactions, two dimensions fall below the critical dimensionality required to sustain such a phase. This renders the experimental realization of 2D spin glasses particularly challenging, though not fundamentally impossible.

Quantum spin liquid states present an equally compelling frontier. Recent reports on monolayer 1T-NbSe₂ and 1T-TaSe₂ suggest signatures of quantum spin liquid behavior [127, 128]; however, a definitive identification of the ground state remains ambiguous. The search for robust quantum spin-liquid signatures in van der Waals materials will undoubtedly occupy a central position in future research.

7.3. Strongly correlated physics in magnetic moiré superlattices

The emergence of flat bands in twisted bilayer vdW antiferromagnets represents a promising frontier for engineering strongly correlated magnetic phases with unprecedented tunability and control. This motivation is anchored in the "magic angle" physics reported in twisted bilayer graphene, where a twist angle of $\sim 1.1^\circ$ stabilizes flat electronic bands [129], which in turn enables superconductivity [130, 131]. Twisted bilayer antiferromagnets similarly promise engineered magnetic correlations with dynamically tunable interaction strengths. Recent first-principles calculations predict the emergence of flat bands and quantum phase transitions from antiferromagnetic to ferromagnetic states in twisted CrSBr bilayers [132]. Furthermore, multiple moiré heterostructures can be investigated, whose interference can generate secondary periodicity with length scales substantially larger than either parent moiré structure. In fact, it has been observed in a twisted (twist angle = $\sim 1.1^\circ$) double bilayer of CrI₃, with a length scale of ~ 300 nm, which spans across multiple parent moiré cells [133].

7.4. Non-equilibrium magnetic control

Creating metastable magnetic states in vdW antiferromagnets and controlling them on timescales of picoseconds to femtoseconds can lead to ultrafast memory devices. One way to access these states is through light-matter coupling; however, future device physics will require a deeper understanding of this interaction, which can be gained through the study of nonlinear optical responses. In particular, recent studies on Co_{1/3}TaS₂ reveal that the nonlinear optical signals are related to their geometric phase and thus can be used to investigate the topological magnetic properties [134].

However, light can heat the sample under study and degrade it. This problem has been solved by Floquet engineering, which has recently gained significant attention and enables the control of a metastable topological state that was previously unreachable under equilibrium conditions. To further extend its capabilities, significant advances in instrumentation are required, particularly in electromagnetic wave sources. Moreover, extending the lifetime of the coherent state will be crucial for manipulating a metastable state for longer [134]. Hence, technological advances in the Floquet method are necessary to realize its full potential.

7.5. Integration into vdW devices

As noted above, the integration of antiferromagnets with other functional materials can enable energy-

and magnetic properties: the Coulomb repulsion U (~ 3 – 8 eV), Hund's coupling J_H (~ 0.8 – 1 eV), crystal-field splitting $10D_q$ (~ 2 – 4 eV), charge-transfer energy Δ (~ 3 – 5 eV), and superexchange J (~ 100 meV). In contrast, van der Waals magnets having chalcogenide and halide elements exhibit substantially different scales: $U \sim 3$ – 8 eV, $J_H \sim 0.8$ – 1 eV, $10D_q \sim 1$ – 3 eV, $\Delta \sim -1$ – 1 eV, and $J \sim 10$ meV.

Among these physical parameters, the most crucial is the charge-transfer energy (Δ) [145–147]. The relative ratio of Δ and U has been used to classify oxides into two regimes: the charge-transfer regime ($\Delta < U$) [148] and the Mott-Hubbard regime ($\Delta > U$) [145]. However, vdW magnets host small or even negative charge-transfer energy due to the relatively closer positioning of ligand p bands to transition-metal d bands compared to those in oxides. This change in Δ requires a more comprehensive picture, namely, the configuration interaction theory developed in the 1980s [149]. This small charge-transfer effect is crucial for a proper understanding of magnetic exciton physics in NiPS₃ [150]. Moreover, charge transfer can also play a crucial role at the interface of a heterostructure, as observed for Fe₃GeTe₂/Cr₂Ge₂Te₆/Fe₃GeTe₂, where coercive fields of the ferromagnetic layers could be selectively controlled by the electric-field-assisted directional charge transfer effect [151]. Although this small or negative charge transfer physics has not been thoroughly examined for other vdW magnets and heterostructures, one should not be surprised to see more fundamental changes to our view of vdW magnets in the future that arise from this.

8. Conclusions

A simple question about the possibility of "magnetic graphene", which was asked in the early 2010s, is the primary driver of the vdW magnets. Since then, they have been extensively studied and constitute an important part of contemporary condensed matter physics research. The major advances enabled by vdW magnets include, but are not limited to, the experimental realization of all three classical spin models (Ising, XY, and Heisenberg) in 2D, gate- and twist-tunable magnetism, the creation and control of non-equilibrium magnetic states using light-matter interactions, and finally, the possibility of their use in practical spintronics applications. We believe that future studies of vdW antiferromagnets will lead to a new phase of the spintronic revolution, given their ultrafast spin dynamics and near-zero stray magnetic fields. However, unlocking the full po-

tential of these magnets requires key technological advances, especially in characterization techniques.

Acknowledgements

We acknowledge Beom Hyun Kim, Kaixuan Zhang, and Giung Park for their helpful discussions and critical comments. We also thank past and present members of the groups for their work, which provides the basis of this review. Last but not least, we are grateful to our collaborators, who, at various stages of our work, have helped shape much of this review. The work was supported by the Leading Researcher Program of the National Research Foundation of Korea (Grant No. RS-2020-NR049405).

References

- [1] K. S. Novoselov, A. K. Geim, S. V. Morozov, D.-e. Jiang, Y. Zhang, S. V. Dubonos, I. V. Grigorieva, A. A. Firsov, Electric field effect in atomically thin carbon films, *science* 306 (5696) (2004) 666–669. doi:<https://doi.org/10.1126/science.1102896>.
- [2] X. Li, X. Wu, J. Yang, Half-metallicity in mnpse3 exfoliated nanosheet with carrier doping, *Journal of the American Chemical Society* 136 (31) (2014) 11065–11069. doi:<https://doi.org/10.1021/ja505097m>.
- [3] N. Sivadas, M. W. Daniels, R. H. Swendsen, S. Okamoto, D. Xiao, Magnetic ground state of semiconducting transition-metal trichalcogenide monolayers, *Physical Review B* 91 (23) (2015) 235425. doi:<https://doi.org/10.1103/PhysRevB.91.235425>.
- [4] J.-G. Park, Opportunities and challenges of 2d magnetic van der waals materials: magnetic graphene?, *Journal of Physics: Condensed Matter* 28 (30) (2016) 301001. doi:[10.1088/0953-8984/28/30/301001](https://doi.org/10.1088/0953-8984/28/30/301001).
- [5] K. S. Novoselov, D. Jiang, F. Schedin, T. Booth, V. Khotkevich, S. Morozov, A. K. Geim, Two-dimensional atomic crystals, *Proceedings of the National Academy of Sciences* 102 (30) (2005) 10451–10453. doi:<https://doi.org/10.1073/pnas.0502848102>.

- [6] B. Radisavljevic, A. Radenovic, J. Brivio, V. Giacometti, A. Kis, Single-layer mos2 transistors, *Nature nanotechnology* 6 (3) (2011) 147–150. doi:<https://doi.org/10.1038/nnano.2010.279>.
- [7] L. Onsager, Crystal statistics. i. a two-dimensional model with an order-disorder transition, *Physical review* 65 (3-4) (1944) 117. doi:<https://doi.org/10.1103/PhysRev.65.117>.
- [8] V. Berezinskii, Destruction of long-range order in one-dimensional and two-dimensional systems having a continuous symmetry group i. classical systems, *Sov. Phys. JETP* 32 (3) (1971) 493–500.
- [9] J. M. Kosterlitz, D. J. Thouless, Ordering, metastability and phase transitions in two-dimensional systems, *Journal of Physics C: Solid State Physics* 6 (7) (1973) 1181. doi:<https://doi.org/10.1088/0022-3719/6/7/010>.
- [10] N. D. Mermin, H. Wagner, Absence of ferromagnetism or antiferromagnetism in one-or two-dimensional isotropic heisenberg models, *Physical Review Letters* 17 (22) (1966) 1133. doi:<https://doi.org/10.1103/PhysRevLett.17.1133>.
- [11] J.-U. Lee, S. Lee, J. H. Ryoo, S. Kang, T. Y. Kim, P. Kim, C.-H. Park, J.-G. Park, H. Cheong, Ising-type magnetic ordering in atomically thin feps3, *Nano letters* 16 (12) (2016) 7433–7438. doi:<https://doi.org/10.1021/acs.nanolett.6b03052>.
- [12] P. Park, Y.-G. Kang, J. Kim, K. H. Lee, H.-J. Noh, M. J. Han, J.-G. Park, Field-tunable toroidal moment and anomalous hall effect in noncollinear antiferromagnetic weyl semimetal col3tas2, *npj Quantum Materials* 7 (1) (2022) 42. doi:<https://doi.org/10.1038/s41535-022-00449-3>.
- [13] B. R. Ortiz, L. C. Gomes, J. R. Morey, M. Winiarski, M. Bordelon, J. S. Mangum, I. W. Oswald, J. A. Rodriguez-Rivera, J. R. Neilson, S. D. Wilson, et al., New kagome prototype materials: discovery of kv3sb5, rbv3sb5, and csv3sb5, *Physical Review Materials* 3 (9) (2019) 094407. doi:<https://doi.org/10.1103/PhysRevMaterials.3.094407>.
- [14] S. Lee, S. Choi, J. Kim, H. Sim, C. Won, S. Lee, S. A. Kim, N. Hur, J.-G. Park, Antiferromagnetic ordering in li2mno3 single crystals with a two-dimensional honeycomb lattice, *Journal of Physics: Condensed Matter* 24 (45) (2012) 456004. doi:<https://doi.org/10.1088/0953-8984/24/45/456004>.
- [15] R. Brec, Review on structural and chemical properties of transition metal phosphorous trisulfides mps3, *Solid State Ionics* 22 (1) (1986) 3–30. doi:[https://doi.org/10.1016/0167-2738\(86\)90055-X](https://doi.org/10.1016/0167-2738(86)90055-X).
- [16] K.-z. Du, X.-z. Wang, Y. Liu, P. Hu, M. I. B. Utama, C. K. Gan, Q. Xiong, C. Kloc, Weak van der waals stacking, wide-range band gap, and raman study on ultrathin layers of metal phosphorus trichalcogenides, *ACS nano* 10 (2) (2016) 1738–1743. doi:<https://doi.org/10.1021/acsnano.5b05927>.
- [17] C.-T. Kuo, M. Neumann, K. Balamurugan, H. J. Park, S. Kang, H. W. Shiu, J. H. Kang, B. H. Hong, M. Han, T. W. Noh, et al., Exfoliation and raman spectroscopic fingerprint of few-layer nips3 van der waals crystals, *Scientific reports* 6 (1) (2016) 20904. doi:<https://doi.org/10.1038/srep20904>.
- [18] S. Lee, K.-Y. Choi, S. Lee, B. H. Park, J.-G. Park, Tunneling transport of mono-and few-layers magnetic van der waals mnps3, *APL Materials* 4 (8) (2016). doi:<https://doi.org/10.1063/1.4961211>.
- [19] G. Ouvrard, R. Brec, J. Rouxel, Structural determination of some mps3 layered phases (m=mn, fe, co, ni and cd), *Materials research bulletin* 20 (10) (1985) 1181–1189. doi:[https://doi.org/10.1016/0025-5408\(85\)90092-3](https://doi.org/10.1016/0025-5408(85)90092-3).
- [20] P. Joy, S. Vasudevan, Magnetism in the layered transition-metal thiophosphates mps3 (m=mn, fe, and ni), *Physical Review B* 46 (9) (1992) 5425. doi:<https://doi.org/10.1103/PhysRevB.46.5425>.
- [21] T. Y. Kim, C.-H. Park, Magnetic anisotropy and magnetic ordering of transition-metal phosphorus trisulfides, *Nano Letters* 21 (23) (2021) 10114–10121. doi:<https://doi.org/10.1021/acs.nanolett.1c03992>.

- [22] Y. Lee, S. Son, C. Kim, S. Kang, J. Shen, M. Kenzelmann, B. Delley, T. Savchenko, S. Parchenko, W. Na, et al., Giant magnetic anisotropy in the atomically thin van der waals antiferromagnet feps3, *Advanced Electronic Materials* 9 (2) (2023) 2200650. doi:<https://doi.org/10.1002/aelm.202200650>.
- [23] D. Lançon, H. Walker, E. Ressouche, B. Ouladiaz, K. Rule, G. McIntyre, T. Hicks, H. M. Rønnow, A. Wildes, Magnetic structure and magnon dynamics of the quasi-two-dimensional antiferromagnet feps 3, *Physical Review B* 94 (21) (2016) 214407. doi:<https://doi.org/10.1103/PhysRevB.94.214407>.
- [24] Y. Lee, C. Kim, S. Son, J. Cui, G. Park, K.-X. Zhang, S. Oh, H. Cheong, A. Kleibert, J.-G. Park, Imaging thermally fluctuating néel vectors in van der waals antiferromagnet nips3, *Nano Letters* 24 (20) (2024) 6043–6050. doi:<https://doi.org/10.1021/acs.nanolett.4c00804>.
- [25] D. Afanasiev, J. R. Hortensius, M. Matthiesen, S. Mañas-Valero, M. Šiškins, M. Lee, E. Lesne, H. S. van Der Zant, P. G. Steeneken, B. A. Ivanov, et al., Controlling the anisotropy of a van der waals antiferromagnet with light, *Science advances* 7 (23) (2021) eabf3096. doi:<https://doi.org/10.1126/sciadv.abf3096>.
- [26] M. J. Coak, D. M. Jarvis, H. Hamidov, C. Haines, P. L. Alireza, C. Liu, S. Son, I. Hwang, G. I. Lampronti, D. Daisenberger, et al., Tuning dimensionality in van-der-waals antiferromagnetic mott insulators tmps3, *Journal of Physics: Condensed Matter* 32 (12) (2019) 124003. doi:<https://doi.org/10.1088/1361-648X/ab5be8>.
- [27] F. Wang, T. A. Shifa, P. Yu, P. He, Y. Liu, F. Wang, Z. Wang, X. Zhan, X. Lou, F. Xia, et al., New frontiers on van der waals layered metal phosphorous trichalcogenides, *Advanced Functional Materials* 28 (37) (2018) 1802151. doi:<https://doi.org/10.1002/adfm.201802151>.
- [28] A. Scheie, P. Park, J. W. Villanova, G. E. Granroth, C. L. Sarkis, H. Zhang, M. B. Stone, J.-G. Park, S. Okamoto, T. Berlijn, et al., Spin wave hamiltonian and anomalous scattering in nips 3, *Physical Review B* 108 (10) (2023) 104402. doi:<https://doi.org/10.1103/PhysRevB.108.104402>.
- [29] A. Wildes, B. Roessli, B. Lebech, K. Godfrey, Spin waves and the critical behaviour of the magnetization in, *Journal of Physics: Condensed Matter* 10 (28) (1998) 6417. doi:<https://doi.org/10.1088/0953-8984/10/28/020>.
- [30] T. Olsen, Magnetic anisotropy and exchange interactions of two-dimensional feps3, nips3 and mnps3 from first principles calculations, *Journal of Physics D: Applied Physics* 54 (31) (2021) 314001. doi:[10.1088/1361-6463/ac000e](https://doi.org/10.1088/1361-6463/ac000e).
- [31] Q. H. Wang, A. Bedoya-Pinto, M. Blei, A. H. Dismukes, A. Hamo, S. Jenkins, M. Koperski, Y. Liu, Q.-C. Sun, E. J. Telford, et al., The magnetic genome of two-dimensional van der waals materials, *ACS nano* 16 (5) (2022) 6960–7079. doi:<https://doi.org/10.1021/acsnano.1c09150>.
- [32] A. C. Ferrari, D. M. Basko, Raman spectroscopy as a versatile tool for studying the properties of graphene, *Nature nanotechnology* 8 (4) (2013) 235–246. doi:<https://doi.org/10.1038/nnano.2013.46>.
- [33] X. Zhang, X.-F. Qiao, W. Shi, J.-B. Wu, D.-S. Jiang, P.-H. Tan, Phonon and raman scattering of two-dimensional transition metal dichalcogenides from monolayer, multilayer to bulk material, *Chemical Society Reviews* 44 (9) (2015) 2757–2785. doi:<https://doi.org/10.1039/C4CS00282B>.
- [34] P. Fleury, R. Loudon, Scattering of light by one- and two-magnon excitations, *Physical Review* 166 (2) (1968) 514. doi:<https://doi.org/10.1103/PhysRev.166.514>.
- [35] M. Bernasconi, G. Marra, G. Benedek, L. Miglio, M. Jouanne, C. Julien, M. Scagliotti, M. Balkanski, Lattice dynamics of layered mp x 3 (m = mn, fe, ni, zn; x = s, se) compounds, *Physical Review B* 38 (17) (1988) 12089. doi:<https://doi.org/10.1103/PhysRevB.38.12089>.
- [36] M. Scagliotti, M. Jouanne, M. Balkanski, G. Ouvrard, Spin dependent phonon raman scattering in antiferromagnetic feps3 layer-type compound, *Solid state communications* 54 (3) (1985) 291–294. doi:[https://doi.org/10.1016/0038-1098\(85\)91087-7](https://doi.org/10.1016/0038-1098(85)91087-7).

- [37] M. Scagliotti, M. Jouanne, M. Balkanski, G. Ouvrard, G. Benedek, Raman scattering in antiferromagnetic feps3 and fepse3 crystals, *Physical Review B* 35 (13) (1987) 7097. doi:<https://doi.org/10.1103/PhysRevB.35.7097>.
- [38] M. Balkanski, M. Jouanne, M. Scagliotti, Magnetic ordering induced raman scattering in feps3 and nips3 layered compounds, *Pure and Applied Chemistry* 59 (10) (1987) 1247–1252. doi:<https://doi.org/10.1351/pac198759101247>.
- [39] W. Jin, H. H. Kim, Z. Ye, S. Li, P. Rezaie, F. Diaz, S. Siddiq, E. Wauer, B. Yang, C. Li, et al., Raman fingerprint of two terahertz spin wave branches in a two-dimensional honeycomb ising ferromagnet, *Nature communications* 9 (1) (2018) 5122. doi:<https://doi.org/10.1038/s41467-018-07547-6>.
- [40] Y. Tian, M. J. Gray, H. Ji, R. J. Cava, K. S. Burch, Magneto-elastic coupling in a potential ferromagnetic 2d atomic crystal, *2D Materials* 3 (2) (2016) 025035. doi:<https://doi.org/10.1088/2053-1583/3/2/025035>.
- [41] H. Chu, C. J. Roh, J. O. Island, C. Li, S. Lee, J. Chen, J.-G. Park, A. F. Young, J. S. Lee, D. Hsieh, Linear magnetoelectric phase in ultrathin mnps3 probed by optical second harmonic generation, *Physical review letters* 124 (2) (2020) 027601. doi:<https://doi.org/10.1103/PhysRevLett.124.027601>.
- [42] K. Kim, S. Y. Lim, J. Kim, J.-U. Lee, S. Lee, P. Kim, K. Park, S. Son, C.-H. Park, J.-G. Park, et al., Antiferromagnetic ordering in van der waals 2d magnetic material mnps3 probed by raman spectroscopy, *2D Materials* 6 (4) (2019) 041001. doi:<https://doi.org/10.1088/2053-1583/ab27d5>.
- [43] H. Ju, Y. Lee, K.-T. Kim, I. H. Choi, C. J. Roh, S. Son, P. Park, J. H. Kim, T. S. Jung, J. H. Kim, et al., Possible persistence of multiferroic order down to bilayer limit of van der waals material nii2, *Nano letters* 21 (12) (2021) 5126–5132. doi:<https://doi.org/10.1021/acs.nanolett.1c01095>.
- [44] Q. Song, C. A. Occhialini, E. Ergeçen, B. Ilyas, D. Amoroso, P. Barone, J. Kapeghian, K. Watanabe, T. Taniguchi, A. S. Botana, et al., Evidence for a single-layer van der waals multiferroic, *Nature* 602 (7898) (2022) 601–605. doi:<https://doi.org/10.1038/s41586-021-04337-x>.
- [45] Q. Zhang, K. Hwangbo, C. Wang, Q. Jiang, J.-H. Chu, H. Wen, D. Xiao, X. Xu, Observation of giant optical linear dichroism in a zigzag antiferromagnet feps3, *Nano Letters* 21 (16) (2021) 6938–6945. doi:<https://doi.org/10.1021/acs.nanolett.1c02188>.
- [46] B. Li, L. Li, Z. Li, F. Wu, J. Cui, X. Cai, F. Liu, Q. Zhang, Resolving spin orientation in the van der waals antiferromagnet crcl3 via the exciton-enhanced magneto-optical voigt effect, *ACS nano* 19 (27) (2025) 25395–25402. doi:<https://doi.org/10.1021/acsnano.5c06978>.
- [47] M. Serri, G. Cucinotta, L. Poggini, G. Serrano, P. Sainctavit, J. Strychalska-Nowak, A. Politano, F. Bonaccorso, A. Caneschi, R. J. Cava, et al., Enhancement of the magnetic coupling in exfoliated crcl3 crystals observed by low-temperature magnetic force microscopy and x-ray magnetic circular dichroism, *Advanced Materials* 32 (24) (2020) 2000566. doi:<https://doi.org/10.1002/adma.202000566>.
- [48] Y.-X. Wang, T. K. Graham, R. Rama-Eiroa, M. A. Islam, M. H. Badarneh, R. Nunes Gontijo, G. P. Tiwari, T. Adhikari, X.-Y. Zhang, K. Watanabe, et al., Configurable antiferromagnetic domains and lateral exchange bias in atomically thin crps4, *Nature Materials* (2025) 1–10doi:<https://doi.org/10.1038/s41563-025-02259-x>.
- [49] I. Schmid, M. Marioni, P. Kappenberger, S. Romer, M. Parlinska-Wojtan, H. Hug, O. Hellwig, M. Carey, E. Fullerton, Exchange bias and domain evolution at 10 nm scales, *Physical review letters* 105 (19) (2010) 197201. doi:<https://doi.org/10.1103/PhysRevLett.105.197201>.
- [50] A. Moser, M. Xiao, P. Kappenberger, K. Takano, W. Weresin, Y. Ikeda, H. Do, H. Hug, High-resolution magnetic force microscopy study of high-density transitions in perpendicular recording media, *Journal of magnetism and magnetic materials* 287 (2005) 298–302. doi:<https://doi.org/10.1016/j.jmmm.2004.10.048>.

- [51] E. Marchiori, L. Ceccarelli, N. Rossi, L. Lorenzelli, C. L. Degen, M. Poggio, Nanoscale magnetic field imaging for 2d materials, *Nature Reviews Physics* 4 (1) (2022) 49–60. doi:<https://doi.org/10.1038/s42254-021-00380-9>.
- [52] A. Farhan, P. Derlet, A. Kleibert, A. Balan, R. Chopdekar, M. Wyss, L. Anghinolfi, F. Nolting, L. J. Heyderman, Exploring hyper-cubic energy landscapes in thermally active finite artificial spin-ice systems, *Nature Physics* 9 (6) (2013) 375–382. doi:<https://doi.org/10.1038/nphys2613>.
- [53] A. Fraile Rodríguez, A. Kleibert, J. Bansmann, A. Voitkans, L. Heyderman, F. Nolting, Size-dependent spin structures in iron nanoparticles, *Physical review letters* 104 (12) (2010) 127201. doi:<https://doi.org/10.1103/PhysRevLett.104.127201>.
- [54] F. Nolting, A. Scholl, J. Stöhr, J. W. Seo, J. Fompeyrine, H. Siegwart, J.-P. Locquet, S. Anders, J. Lüning, E. Fullerton, et al., Direct observation of the alignment of ferromagnetic spins by antiferromagnetic spins, *Nature* 405 (6788) (2000) 767–769. doi:<https://doi.org/10.1038/35015515>.
- [55] A. Gruber, A. Drabenstedt, C. Tietz, L. Fleury, J. Wrachtrup, C. v. Borzyskowski, Scanning confocal optical microscopy and magnetic resonance on single defect centers, *Science* 276 (5321) (1997) 2012–2014. doi:<https://doi.org/10.1126/science.276.5321.2012>.
- [56] R. Schirhagl, K. Chang, M. Loretz, C. L. Degen, Nitrogen-vacancy centers in diamond: nanoscale sensors for physics and biology, *Annual review of physical chemistry* 65 (1) (2014) 83–105. doi:<https://doi.org/10.1146/annurev-physchem-040513-103659>.
- [57] A. Ariyaratne, D. Bluvstein, B. A. Myers, A. C. B. Jayich, Nanoscale electrical conductivity imaging using a nitrogen-vacancy center in diamond, *Nature communications* 9 (1) (2018) 2406. doi:<https://doi.org/10.1038/s41467-018-04798-1>.
- [58] K. Chang, A. Eichler, J. Rhensius, L. Lorenzelli, C. L. Degen, Nanoscale imaging of current density with a single-spin magnetometer, *Nano letters* 17 (4) (2017) 2367–2373. doi:<https://doi.org/10.1021/acs.nanolett.6b05304>.
- [59] U. Vool, A. Hamo, G. Varnavides, Y. Wang, T. X. Zhou, N. Kumar, Y. Dovzhenko, Z. Qiu, C. A. Garcia, A. T. Pierce, et al., Imaging phonon-mediated hydrodynamic flow in wte2, *Nature Physics* 17 (11) (2021) 1216–1220. doi:<https://doi.org/10.1038/s41567-021-01341-w>.
- [60] C. S. Wolfe, V. P. Bhallamudi, H. L. Wang, C. H. Du, S. Manuilov, R. Teeling-Smith, A. Berger, R. Adur, F. Yang, P. C. Hammel, Off-resonant manipulation of spins in diamond via precessing magnetization of a proximal ferromagnet, *Physical Review B* 89 (18) (2014) 180406. doi:<https://doi.org/10.1103/PhysRevB.89.180406>.
- [61] T. Van der Sar, F. Casola, R. Walsworth, A. Yacoby, Nanometre-scale probing of spin waves using single electron spins, *Nature communications* 6 (1) (2015) 7886. doi:<https://doi.org/10.1038/ncomms8886>.
- [62] I. Bertelli, J. J. Carmiggelt, T. Yu, B. G. Simon, C. C. Pothoven, G. E. Bauer, Y. M. Blanter, J. Aarts, T. Van Der Sar, Magnetic resonance imaging of spin-wave transport and interference in a magnetic insulator, *Science advances* 6 (46) (2020) eabd3556. doi:<https://doi.org/10.1126/sciadv.abd3556>.
- [63] G. A. Álvarez, D. Suter, Measuring the spectrum of colored noise by dynamical decoupling, *Physical review letters* 107 (23) (2011) 230501. doi:<https://doi.org/10.1103/PhysRevLett.107.230501>.
- [64] C. L. Degen, F. Reinhard, P. Cappellaro, Quantum sensing, *Reviews of modern physics* 89 (3) (2017) 035002. doi:<https://doi.org/10.1103/RevModPhys.89.035002>.
- [65] J. G. Park, Magnetic van der Waals material: opportunities and challenges, in: *Proceedings of the Korean Physical Society Fall Meeting, 2015*.
- [66] J. G. Park, New opportunities of magnetic graphene TMPX₃, Talk presented at the 16th Japan-Korea-Taiwan Symposium on Strongly Correlated Electron System, university of Tokyo, Japan (2016).

- [67] J.-G. Park, K. Zhang, H. Cheong, J. H. Kim, C. Belvin, D. Hsieh, H. Ning, N. Gedik, 2d van der waals magnets: from fundamental physics to applications, arXiv preprint arXiv:2505.02355 (2025). doi:<https://doi.org/10.48550/arXiv.2505.02355>.
- [68] C. Gong, L. Li, Z. Li, H. Ji, A. Stern, Y. Xia, T. Cao, W. Bao, C. Wang, Y. Wang, et al., Discovery of intrinsic ferromagnetism in two-dimensional van der waals crystals, *Nature* 546 (7657) (2017) 265–269. doi:<https://doi.org/10.1038/nature22060>.
- [69] B. Huang, G. Clark, E. Navarro-Moratalla, D. R. Klein, R. Cheng, K. L. Seyler, D. Zhong, E. Schmidgall, M. A. McGuire, D. H. Cobden, et al., Layer-dependent ferromagnetism in a van der waals crystal down to the monolayer limit, *Nature* 546 (7657) (2017) 270–273. doi:<https://doi.org/10.1038/nature22391>.
- [70] D. R. Klein, D. MacNeill, J. L. Lado, D. Soriano, E. Navarro-Moratalla, K. Watanabe, T. Taniguchi, S. Manni, P. Canfield, J. Fernández-Rossier, et al., Probing magnetism in 2d van der waals crystalline insulators via electron tunneling, *Science* 360 (6394) (2018) 1218–1222. doi:<https://doi.org/10.1126/science.aar3617>.
- [71] T. Song, X. Cai, M. W.-Y. Tu, X. Zhang, B. Huang, N. P. Wilson, K. L. Seyler, L. Zhu, T. Taniguchi, K. Watanabe, et al., Giant tunneling magnetoresistance in spin-filter van der waals heterostructures, *Science* 360 (6394) (2018) 1214–1218. doi:<https://doi.org/10.1126/science.aar4851>.
- [72] Y. Deng, Y. Yu, Y. Song, J. Zhang, N. Z. Wang, Z. Sun, Y. Yi, Y. Z. Wu, S. Wu, J. Zhu, et al., Gate-tunable room-temperature ferromagnetism in two-dimensional fe₃gete₂, *Nature* 563 (7729) (2018) 94–99. doi:<https://doi.org/10.1038/s41586-018-0626-9>.
- [73] Q. Tong, F. Liu, J. Xiao, W. Yao, Skyrmions in the moiré of van der waals 2d magnets, *Nano letters* 18 (11) (2018) 7194–7199. doi:<https://doi.org/10.1021/acs.nanolett.8b03315>.
- [74] K. Hejazi, Z.-X. Luo, L. Balents, Noncollinear phases in moiré magnets, *Proceedings of the National Academy of Sciences* 117 (20) (2020) 10721–10726. doi:<https://doi.org/10.1073/pnas.2000347117>.
- [75] Y. Xu, A. Ray, Y.-T. Shao, S. Jiang, K. Lee, D. Weber, J. E. Goldberger, K. Watanabe, T. Taniguchi, D. A. Muller, et al., Coexisting ferromagnetic–antiferromagnetic state in twisted bilayer cri₃, *Nature nanotechnology* 17 (2) (2022) 143–147. doi:<https://doi.org/10.1038/s41565-021-01014-y>.
- [76] K. Kim, S. Y. Lim, J.-U. Lee, S. Lee, T. Y. Kim, K. Park, G. S. Jeon, C.-H. Park, J.-G. Park, H. Cheong, Suppression of magnetic ordering in xxz-type antiferromagnetic monolayer nips₃, *Nature communications* 10 (1) (2019) 345. doi:<https://doi.org/10.1038/s41467-018-08284-6>.
- [77] A. Wildes, V. Simonet, E. Ressouche, R. Ballou, G. McIntyre, The magnetic properties and structure of the quasi-two-dimensional antiferromagnet cops₃, *Journal of Physics: Condensed Matter* 29 (45) (2017) 455801. doi:<https://doi.org/10.1088/1361-648X/aa8a43>.
- [78] C. Autieri, G. Cuono, C. Noce, M. Rybak, K. M. Kotur, C. E. Agrapidis, K. Wohlfeld, M. Birowska, Limited ferromagnetic interactions in monolayers of mps₃ (m = mn and ni), *The Journal of Physical Chemistry C* 126 (15) (2022) 6791–6802. doi:<https://doi.org/10.1021/acs.jpcc.2c00646>.
- [79] R. Mikhaylovskiy, T. Huisman, A. Popov, A. Zvezdin, T. Rasing, R. Pisarev, A. Kimel, Terahertz magnetization dynamics induced by femtosecond resonant pumping of dy 3+ subsystem in the multisublattice antiferromagnet dyfeo 3, *Physical Review B* 92 (9) (2015) 094437. doi:<https://doi.org/10.1103/PhysRevB.92.094437>.
- [80] S. Baierl, M. Hohenleutner, T. Kampfrath, A. Zvezdin, A. Kimel, R. Huber, R. Mikhaylovskiy, Nonlinear spin control by terahertz-driven anisotropy fields, *Nature Photonics* 10 (11) (2016) 715–718. doi:<https://doi.org/10.1038/nphoton.2016.181>.
- [81] R. Iida, T. Satoh, T. Shimura, K. Kuroda, B. Ivanov, Y. Tokunaga, Y. Tokura, Spectral dependence of photoinduced spin precession in dyfeo 3, *Physical Review B—Condensed*

- Matter and Materials Physics 84 (6) (2011) 064402. doi:<https://doi.org/10.1103/PhysRevB.84.064402>.
- [82] R. Mikhaylovskiy, T. Huisman, V. Gavrichkov, S. Polukeev, S. Ovchinnikov, D. Afanasiev, R. Pisarev, T. Rasing, A. Kimel, Resonant pumping of d-d crystal field electronic transitions as a mechanism of ultrafast optical control of the exchange interactions in iron oxides, *Physical review letters* 125 (15) (2020) 157201. doi:<https://doi.org/10.1103/PhysRevLett.125.157201>.
- [83] B. Ilyas, T. Luo, A. von Hoegen, E. Viñas Boström, Z. Zhang, J. Park, J. Kim, J.-G. Park, K. A. Nelson, A. Rubio, et al., Terahertz field-induced metastable magnetization near criticality in feps3, *Nature* 636 (8043) (2024) 609–614. doi:<https://doi.org/10.1038/s41586-024-08226-x>.
- [84] N. Chandrasekharan, S. Vasudevan, Magnetism and exchange in the layered antiferromagnets, *Journal of Physics: Condensed Matter* 6 (24) (1994) 4569. doi:<https://doi.org/10.1088/0953-8984/6/24/017>.
- [85] D. Basov, R. Averitt, D. Hsieh, Towards properties on demand in quantum materials, *Nature materials* 16 (11) (2017) 1077–1088. doi:<https://doi.org/10.1038/nmat5017>.
- [86] T. Oka, S. Kitamura, Floquet engineering of quantum materials, *Annual Review of Condensed Matter Physics* 10 (1) (2019) 387–408. doi:<https://doi.org/10.1146/annurev-conmatphys-031218-013423>.
- [87] J.-Y. Shan, M. Ye, H. Chu, S. Lee, J.-G. Park, L. Balents, D. Hsieh, Giant modulation of optical nonlinearity by floquet engineering, *Nature* 600 (7888) (2021) 235–239. doi:<https://doi.org/10.1038/s41586-021-04051-8>.
- [88] C. Wang, Y. Gao, H. Lv, X. Xu, D. Xiao, Stacking domain wall magnons in twisted van der waals magnets, *Physical Review Letters* 125 (24) (2020) 247201. doi:<https://doi.org/10.1103/PhysRevLett.125.247201>.
- [89] T. Song, Q.-C. Sun, E. Anderson, C. Wang, J. Qian, T. Taniguchi, K. Watanabe, M. A. McGuire, R. Stöhr, D. Xiao, et al., Direct visualization of magnetic domains and moiré magnetism in twisted 2d magnets, *Science* 374 (6571) (2021) 1140–1144. doi:<https://doi.org/10.1126/science.abj7478>.
- [90] B. Zhang, P. Lu, R. Tabrizian, P. X.-L. Feng, Y. Wu, 2d magnetic heterostructures: Spintronics and quantum future, *npj Spintronics* 2 (1) (2024) 6. doi:<https://doi.org/10.1038/s44306-024-00011-w>.
- [91] T. Su, M. Lohmann, J. Li, Y. Xu, B. Niu, M. Alghamdi, H. Zhou, Y. Cui, R. Cheng, T. Taniguchi, et al., Current-induced c13 surface spin-flop transition probed by proximity magnetoresistance in pt, *2D Materials* 7 (4) (2020) 045006. doi:<https://doi.org/10.1088/2053-1583/ab9dd5>.
- [92] C. Ye, X. Xie, W. Lv, K. Huang, A. J. Yang, S. Jiang, X. Liu, D. Zhu, X. Qiu, M. Tong, et al., Nonreciprocal transport in a bilayer of mnbi2te4 and pt, *Nano Letters* 22 (3) (2022) 1366–1373. doi:<https://doi.org/10.1021/acs.nanolett.1c04756>.
- [93] M. Lohmann, T. Su, B. Niu, Y. Hou, M. Alghamdi, M. Aldosary, W. Xing, J. Zhong, S. Jia, W. Han, et al., Probing magnetism in insulating cr2ge2te6 by induced anomalous hall effect in pt, *Nano letters* 19 (4) (2019) 2397–2403. doi:<https://doi.org/10.1021/acs.nanolett.8b05121>.
- [94] Y. Ma, S. Xu, Z. Chen, C. Liu, T. Yang, Y. Yan, J. Z. Liu, F. Xue, X. Zhang, The van der waals antiferromagnetic proximity effect at the feps 3/pt uncompensated interface, *Materials Horizons* (2025). doi:<https://doi.org/10.1039/D5MH00023H>.
- [95] J. Kim, K.-X. Zhang, P. Park, W. Cho, H. Kim, H.-J. Noh, J.-G. Park, Electrical control of topological 3q state in intercalated van der waals antiferromagnet cox-tas2, *Nature Communications* 16 (1) (2025) 8943. doi:<https://doi.org/10.1038/s41467-025-63991-1>.
- [96] K.-X. Zhang, S. Lee, W. Cho, J.-G. Park, Current-driven switching of topological spin chirality in a van der waals antiferromagnet, *arXiv preprint arXiv:2511.14241* (2025). doi:<https://doi.org/10.48550/arXiv.2511.14241>.
- [97] R. Zhu, W. Zhang, W. Shen, P. K. J. Wong, Q. Wang, Q. Liang, Z. Tian, Y. Zhai, C.-w.

- Qiu, A. T. Wee, Exchange bias in van der waals $\text{CrI}_3/\text{Fe}_3\text{GeTe}_2$ heterostructures, *Nano Letters* 20 (7) (2020) 5030–5035. doi:<https://doi.org/10.1021/acs.nanolett.0c01149>.
- [98] G. Hu, Y. Zhu, J. Xiang, T.-Y. Yang, M. Huang, Z. Wang, Z. Wang, P. Liu, Y. Zhang, C. Feng, et al., Antisymmetric magnetoresistance in a van der waals antiferromagnetic/ferromagnetic layered $\text{MnPS}_3/\text{Fe}_3\text{GeTe}_2$ stacking heterostructure, *ACS nano* 14 (9) (2020) 12037–12044. doi:<https://doi.org/10.1021/acsnano.0c05252>.
- [99] H. Dai, H. Cheng, M. Cai, Q. Hao, Y. Xing, H. Chen, X. Chen, X. Wang, J.-B. Han, Enhancement of the coercive field and exchange bias effect in $\text{Fe}_3\text{GeTe}_2/\text{MnPx}_3$ ($x = s$ and se) van der waals heterostructures, *ACS Applied Materials & Interfaces* 13 (20) (2021) 24314–24320. doi:<https://doi.org/10.1021/acssami.1c05265>.
- [100] S. Albarakati, W.-Q. Xie, C. Tan, G. Zheng, M. Algarni, J. Li, J. Partridge, M. J. Spencer, L. Farrar, Y. Xiong, et al., Electric control of exchange bias effect in $\text{FePS}_3\text{-Fe}_5\text{GeTe}_2$ van der waals heterostructures, *Nano Letters* 22 (15) (2022) 6166–6172. doi:<https://doi.org/10.1021/acs.nanolett.2c01370>.
- [101] L. Wei, Y. Chen, L. Chen, P. Liu, W. Niu, L. Zhang, Y. Pu, Exchange bias effect in the total two-dimensional van der waals heterostructures of $\text{Fe}_5\text{-xGeTe}_2/\text{CrPS}_4$, *Journal of Applied Physics* 137 (13) (2025). doi:<https://doi.org/10.1063/5.0253775>.
- [102] X. Wang, C. Wang, Y. Wang, C. Ye, A. Rahman, M. Zhang, S. Son, J. Tan, Z. Zhang, W. Ji, et al., Artificially creating emergent interfacial antiferromagnetism and its manipulation in a magnetic van der waals heterostructure, *ACS nano* 19 (8) (2025) 8108–8117. doi:<https://doi.org/10.1021/acsnano.4c16450>.
- [103] E. J. Telford, A. H. Dismukes, K. Lee, M. Cheng, A. Wieteska, A. K. Bartholomew, Y.-S. Chen, X. Xu, A. N. Pasupathy, X. Zhu, et al., Layered antiferromagnetism induces large negative magnetoresistance in the van der waals semiconductor CrSBr , *Advanced Materials* 32 (37) (2020) 2003240. doi:<https://doi.org/10.1002/adma.202003240>.
- [104] C.-T. Chou, E. Park, J. Ingla-Aynes, J. Klein, K. Mosina, J. S. Moodera, Z. Sofer, F. M. Ross, L. Liu, Large magnetoresistance in an electrically tunable van der waals antiferromagnet, *Physical Review Letters* 135 (13) (2025) 136702. doi:<https://doi.org/10.1103/hpmq-rnh4>.
- [105] Y. Chen, K. Samanta, N. A. Shahed, H. Zhang, C. Fang, A. Ernst, E. Y. Tsymlal, S. S. Parkin, Twist-assisted all-antiferromagnetic tunnel junction in the atomic limit, *Nature* 632 (8027) (2024) 1045–1051. doi:<https://doi.org/10.1038/s41586-024-07818-x>.
- [106] W. Jin, G. Zhang, H. Wu, L. Yang, B. Xiao, J. Yu, W. Zhang, H. Chang, Nonvolatile multistate magnetoresistance in all-van der waals antiferromagnet-based spin valves, *Applied Physics Letters* 126 (15) (2025). doi:<https://doi.org/10.1063/5.0253237>.
- [107] P. Shi, X. Wang, L. Zhang, W. Song, K. Yang, S. Wang, R. Zhang, L. Zhang, T. Taniguchi, K. Watanabe, et al., Magnetoresistance oscillations in vertical junctions of 2d antiferromagnetic semiconductor CrPS_4 , *Physical Review X* 14 (4) (2024) 041065. doi:<https://doi.org/10.1103/PhysRevX.14.041065>.
- [108] T. Jungwirth, X. Marti, P. Wadley, J. Wunderlich, Antiferromagnetic spintronics, *Nature nanotechnology* 11 (3) (2016) 231–241. doi:<https://doi.org/10.1103/RevModPhys.90.015005>.
- [109] J. Han, R. Cheng, L. Liu, H. Ohno, S. Fukami, Coherent antiferromagnetic spintronics, *Nature Materials* 22 (6) (2023) 684–695. doi:<https://doi.org/10.1038/s41563-023-01492-6>.
- [110] A. Dal Din, O. Amin, P. Wadley, K. Edmonds, Antiferromagnetic spintronics and beyond, *npj Spintronics* 2 (1) (2024) 25. doi:<https://doi.org/10.1038/s44306-024-00029-0>.
- [111] H. Yan, Z. Feng, P. Qin, X. Zhou, H. Guo, X. Wang, H. Chen, X. Zhang, H. Wu, C. Jiang, et al., Electric-field-controlled antiferromagnetic spintronic devices, *Advanced Materials* 32 (12) (2020) 1905603. doi:<https://doi.org/10.1002/adma.201905603>.
- [112] S. Rahman, J. F. Torres, A. R. Khan, Y. Lu, Recent developments in van der waals antiferromagnetic 2d materials: Synthesis, characterization, and device implementation, *ACS nano*

- 15 (11) (2021) 17175–17213. doi:<https://doi.org/10.1021/acsnano.1c06864>.
- [113] F. Yao, M. Liao, M. Gibertini, C.-Y. Cheon, X. Lin, F. Wu, K. Watanabe, T. Taniguchi, I. Gutiérrez-Lezama, A. F. Morpurgo, Switching on and off the spin polarization of the conduction band in antiferromagnetic bilayer transistors, *Nature Nanotechnology* (2025) 1–8doi:<https://doi.org/10.1038/s41565-025-01872-w>.
- [114] S.-J. Gong, C. Gong, Y.-Y. Sun, W.-Y. Tong, C.-G. Duan, J.-H. Chu, X. Zhang, Electrically induced 2d half-metallic antiferromagnets and spin field effect transistors, *Proceedings of the National Academy of Sciences* 115 (34) (2018) 8511–8516. doi:<https://doi.org/10.1073/pnas.1715465115>.
- [115] G. Liu, S.-H. Ke, Electronic and transport engineering of a-type antiferromagnets with ferroelectric sandwich structure: Toward multistate nonvolatile memory applications, *Nano Letters* 24 (35) (2024) 10776–10782. doi:<https://doi.org/10.1021/acsnanolett.4c01916>.
- [116] G. Zhao, Y. Zhao, Y. Zhang, K. Yang, Z. Guo, J. Liu, T. Zhao, K. Yan, X. Chen, Q. Li, et al., Doping-induced magnetic phase transition enables all-electrical spin control in crsbr, *Nature Communications* (2025). doi:<https://doi.org/10.1038/s41467-025-67561-3>.
- [117] K.-X. Zhang, S. Cheon, H. Kim, P. Park, Y. An, S. Son, J. Cui, J. Keum, J. Choi, Y. Jo, et al., Current-driven collective control of helical spin texture in van der waals antiferromagnet, *Physical Review Letters* 134 (17) (2025) 176701. doi:<https://doi.org/10.1103/PhysRevLett.134.176701>.
- [118] H. Takagi, R. Takagi, S. Minami, T. Nomoto, K. Ohishi, M.-T. Suzuki, Y. Yanagi, M. Hirayama, N. Khanh, K. Karube, et al., Spontaneous topological hall effect induced by non-coplanar antiferromagnetic order in intercalated van der waals materials, *Nature Physics* 19 (7) (2023) 961–968. doi:<https://doi.org/10.1038/s41567-023-02017-3>.
- [119] P. Park, W. Cho, C. Kim, Y. An, Y.-G. Kang, M. Avdeev, R. Sibille, K. Iida, R. Kajimoto, K. H. Lee, et al., Tetrahedral triple-q magnetic ordering and large spontaneous hall conductivity in the metallic triangular antiferromagnet $\text{Co}_1/3\text{TaS}_2$, *Nature Communications* 14 (1) (2023) 8346. doi:<https://doi.org/10.1038/s41467-023-43853-4>.
- [120] Z. Meng, W. Lin, Z. Zhao, B. Zhang, B. Li, Y. Lv, G. Han, S. Li, Y. Cai, F. Jin, et al., Spontaneous topological hall effect in intercalated $\text{Co}_1/3\text{TaS}_2$ nanoflakes with non-coplanar antiferromagnetic order, *Advanced Functional Materials* (2025) 2502016doi:<https://doi.org/10.1002/adfm.202502016>.
- [121] T. Song, Z. Fei, M. Yankowitz, Z. Lin, Q. Jiang, K. Hwangbo, Q. Zhang, B. Sun, T. Taniguchi, K. Watanabe, et al., Switching 2d magnetic states via pressure tuning of layer stacking, *Nature materials* 18 (12) (2019) 1298–1302. doi:<https://doi.org/10.1038/s41563-019-0505-2>.
- [122] T. Li, S. Jiang, N. Sivadas, Z. Wang, Y. Xu, D. Weber, J. E. Goldberger, K. Watanabe, T. Taniguchi, C. J. Fennie, et al., Pressure-controlled interlayer magnetism in atomically thin CrI_3 , *Nature materials* 18 (12) (2019) 1303–1308. doi:<https://doi.org/10.1038/s41563-019-0506-1>.
- [123] K. Binder, A. P. Young, Spin glasses: Experimental facts, theoretical concepts, and open questions, *Reviews of Modern physics* 58 (4) (1986) 801. doi:<https://doi.org/10.1103/RevModPhys.58.801>.
- [124] P. W. Anderson, The resonating valence bond state in La_2CuO_4 and superconductivity, *science* 235 (4793) (1987) 1196–1198. doi:<https://doi.org/10.1126/science.235.4793.1196>.
- [125] L. Hoines, R. Stubi, R. Loloee, J. Cowen, J. Bass, How thin a spin glass is still a spin glass?, *Physical review letters* 66 (9) (1991) 1224. doi:<https://doi.org/10.1103/PhysRevLett.66.1224>.
- [126] I. Morgenstern, K. Binder, Magnetic correlations in two-dimensional spin-glasses, *Physical Review B* 22 (1) (1980) 288. doi:<https://doi.org/10.1103/PhysRevB.22.288>.
- [127] Q. Zhang, W.-Y. He, Y. Zhang, Y. Chen, L. Jia, Y. Hou, H. Ji, H. Yang, T. Zhang, L. Liu, et al., Quantum spin liquid signatures in monolayer 1t-nbse_2 , *Nature Communications*

- 15 (1) (2024) 2336. doi:<https://doi.org/10.1038/s41467-024-46612-1>.
- [128] W. Ruan, Y. Chen, S. Tang, J. Hwang, H.-Z. Tsai, R. L. Lee, M. Wu, H. Ryu, S. Kahn, F. Liou, et al., Evidence for quantum spin liquid behaviour in single-layer $1t\text{-TaS}_2$ from scanning tunnelling microscopy, *Nature Physics* 17 (10) (2021) 1154–1161. doi:<https://doi.org/10.1038/s41567-021-01321-0>.
- [129] Y. Cao, V. Fatemi, A. Demir, S. Fang, S. L. Tomarken, J. Y. Luo, J. D. Sanchez-Yamagishi, K. Watanabe, T. Taniguchi, E. Kaxiras, et al., Correlated insulator behaviour at half-filling in magic-angle graphene superlattices, *Nature* 556 (7699) (2018) 80–84. doi:<https://doi.org/10.1038/nature26154>.
- [130] Y. Cao, V. Fatemi, S. Fang, K. Watanabe, T. Taniguchi, E. Kaxiras, P. Jarillo-Herrero, Unconventional superconductivity in magic-angle graphene superlattices, *Nature* 556 (7699) (2018) 43–50. doi:<https://doi.org/10.1038/nature26160>.
- [131] S. K. Behura, A. Miranda, S. Nayak, K. Johnson, P. Das, N. R. Pradhan, Moiré physics in twisted van der waals heterostructures of 2d materials, *Emergent Materials* 4 (4) (2021) 813–826. doi:<https://doi.org/10.1007/s42247-021-00270-x>.
- [132] J. Liu, X. Zhang, G. Lu, Moiré magnetism and moiré excitons in twisted crsbr bilayers, *Proceedings of the National Academy of Sciences* 122 (1) (2025) e2413326121. doi:<https://doi.org/10.1073/pnas.2413326121>.
- [133] K. C. Wong, R. Peng, E. Anderson, J. Ross, B. Yang, M. Cheng, S. Jayaram, M. Lenger, X. Zhou, Y. T. Kong, et al., Super-moiré spin textures in twisted antiferromagnets, *arXiv preprint arXiv:2510.25545* (2025). doi:<https://doi.org/10.48550/arXiv.2510.25545>.
- [134] C. Bao, P. Tang, D. Sun, S. Zhou, Light-induced emergent phenomena in 2d materials and topological materials, *Nature Reviews Physics* 4 (1) (2022) 33–48. doi:<https://doi.org/10.1038/s42254-021-00388-1>.
- [135] Z. Zheng, T. Zeng, T. Zhao, S. Shi, L. Ren, T. Zhang, L. Jia, Y. Gu, R. Xiao, H. Zhou, et al., Effective electrical manipulation of a topological antiferromagnet by orbital torques, *Nature Communications* 15 (1) (2024) 745. doi:<https://doi.org/10.1038/s41467-024-45109-1>.
- [136] C.-Y. Wang, C. Wang, F. Meng, P. Wang, S. Wang, S.-J. Liang, F. Miao, 2d layered materials for memristive and neuromorphic applications, *Advanced Electronic Materials* 6 (2) (2020) 1901107. doi:<https://doi.org/10.1002/aelm.201901107>.
- [137] A. F. May, M.-H. Du, V. R. Cooper, M. A. McGuire, Tuning magnetic order in the van der waals metal Fe_5GeTe_2 by cobalt substitution, *Physical Review Materials* 4 (7) (2020) 074008. doi:<https://doi.org/10.1103/PhysRevMaterials.4.074008>.
- [138] C. Tian, F. Pan, S. Xu, K. Ai, T. Xia, P. Cheng, Tunable magnetic properties in van der waals crystals ($\text{Fe}_{1-x}\text{Co}_x$) Fe_5GeTe_2 , *Applied Physics Letters* 116 (20) (2020). doi:<https://doi.org/10.1063/5.0006337>.
- [139] H. Zhang, D. Raftrey, Y.-T. Chan, Y.-T. Shao, R. Chen, X. Chen, X. Huang, J. T. Reichenadter, K. Dong, S. Susarla, et al., Room-temperature skyrmion lattice in a layered magnet ($\text{Fe}_0.5\text{Co}_0.5$) Fe_5GeTe_2 , *Science advances* 8 (12) (2022) eabm7103. doi:<https://doi.org/10.1126/sciadv.abm7103>.
- [140] T. Hu, Y. Ma, L. Lu, Y. Deng, M. Wang, K. Zhu, L. Xi, Y. Xiong, X. Kan, G. Wang, et al., Enhanced magnetic transition temperature through ferromagnetic and antiferromagnetic interaction in cobalt-substituted Fe_5GeTe_2 , *Applied Physics Letters* 125 (2) (2024). doi:<https://doi.org/10.1063/5.0213046>.
- [141] L. Lu, Q. Wang, H. Duan, K. Zhu, T. Hu, Y. Ma, S. Shen, Y. Niu, J. Liu, J. Wang, et al., Tunable magnetism in atomically thin itinerant antiferromagnet with room-temperature ferromagnetic order, *Nano Letters* 24 (20) (2024) 5984–5992. doi:<https://doi.org/10.1021/acs.nanolett.4c00472>.
- [142] W.-M. Zhao, Y.-L. Liu, L. Yang, C. Tan, Y. Yang, Z. Zhu, M. Chen, T. Yan, R. Hu, J. Partridge, et al., Interface-controlled antiferromagnetic tunnel junctions based on a metallic van der waals a-type antiferromagnet, *Nature Communications* (2025). doi:<https://doi.org/10.1038/s41467-025-66981-5>.

- [143] J. Tian, C. Wang, L. Zhou, Y. Bai, Y. Yang, Y. Lei, L. Chen, C. Li, J. Wang, Thermal magnon transport in van der waals antiferromagnetic crps4, *Applied Physics Letters* 127 (6) (2025). doi:<https://doi.org/10.1063/5.0286285>.
- [144] X. He, S. Ding, H. G. Giil, J. Wang, M. Bhukta, M. Wu, W. Shi, Z. Lin, Z. Liang, J. Yang, et al., Spin seebeck in the weakly exchange-coupled van der waals antiferromagnet across the spin-flip transition, *Nature Communications* 16 (1) (2025) 3037. doi:<https://doi.org/10.1038/s41467-025-58306-3>.
- [145] J. Zaanen, G. Sawatzky, J. Allen, Band gaps and electronic structure of transition-metal compounds, *Physical review letters* 55 (4) (1985) 418. doi:<https://doi.org/10.1103/PhysRevLett.55.418>.
- [146] D. Khomskii, Unusual valence, negative charge-transfer gaps and self-doping in transition-metal compounds, *arXiv preprint cond-mat/0101164* (2001). doi:<https://doi.org/10.48550/arXiv.cond-mat/0101164>.
- [147] A. Bocquet, T. Mizokawa, K. Morikawa, A. Fujimori, S. Barman, K. Maiti, D. Sarma, Y. Tokura, M. Onoda, Electronic structure of early 3d-transition-metal oxides by analysis of the 2p core-level photoemission spectra, *Physical Review B* 53 (3) (1996) 1161. doi:<https://doi.org/10.1103/PhysRevB.53.1161>.
- [148] A. Bocquet, T. Mizokawa, T. Saitoh, H. Namatame, A. Fujimori, Electronic structure of 3d-transition-metal compounds by analysis of the 2p core-level photoemission spectra, *Physical Review B* 46 (7) (1992) 3771. doi:<https://doi.org/10.1103/PhysRevB.46.3771>.
- [149] D. De Boer, C. Haas, G. Sawatzky, Exciton satellites in photoelectron spectra, *Physical Review B* 29 (8) (1984) 4401. doi:<https://doi.org/10.1103/PhysRevB.29.4401>.
- [150] S. Kang, K. Kim, B. H. Kim, J. Kim, K. I. Sim, J.-U. Lee, S. Lee, K. Park, S. Yun, T. Kim, et al., Coherent many-body exciton in van der waals antiferromagnet nips3, *Nature* 583 (7818) (2020) 785–789. doi:<https://doi.org/10.1038/s41586-020-2520-5>.
- [151] Z.-A. Wang, W. Xue, F. Yan, W. Zhu, Y. Liu, X. Zhang, Z. Wei, K. Chang, Z. Yuan, K. Wang, Selectively controlled ferromagnets by electric fields in van der waals ferromagnetic heterojunctions, *Nano Letters* 23 (2) (2023) 710–717. doi:<https://doi.org/10.1021/acs.nanolett.2c04796>.